ΕΛΛΗΝΙΚΗ ΔΗΜΟΚΡΑΤΙΑ
Εθνικόν και Καποδιστριακόν Πανεπιστήμιον Αθηνών
ΙΔΡΥΘΕΝ ΤΟ 1837

NATIONAL & KAPODISTRIAN UNIVERSITY OF ATHENS
SCHOOL OF HEALTH SCIENCES
SCHOOL OF MEDICINE & DEPARTMENT OF PHARMACY
INTERDISCIPLINARY POSTGRADUATE PROGRAM:
"NANOMEDICINE"

Master Thesis

"Polymer micellar nanostructures encapsulating bioimaging agents."

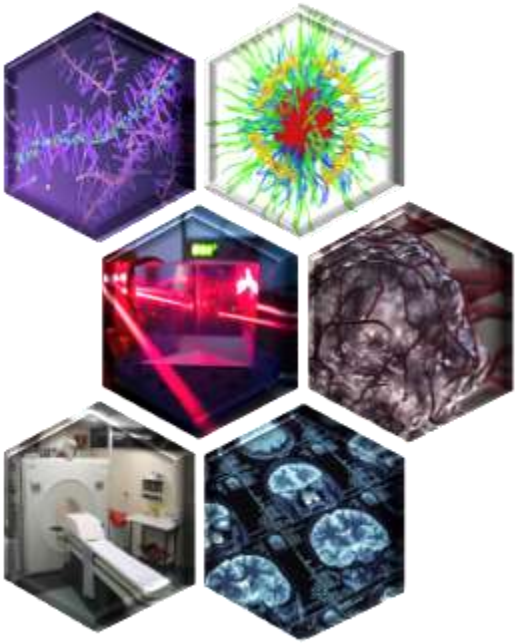

Anargyros Drolapas, *Chemical Engineer*

Supervisor:
Dr. Stergios Pispas

Committee Members:
Prof. Natassa Pippa
Prof. Nefeli Lagopati

Athens, June 2024

Abstract

Block Copolymer Micelles (BCPs) are a novel class of nanomaterials (5-100 nm) with outstanding properties and promising applications in medical imaging. Their exceptional colloidal stability in biological media affords particulate systems with enhanced chemical stability and long circulation times in the human body. Besides the above, BCP micelles are known for their structural versatility and their ability to host multiple contrast agents (CAs) in their hydrophobic core or in their hydrophilic corona. The types of CAs that can be incorporated in BCP micelles range from fluorophores for fluorescence imaging to gadolinium-based CAs or superparamagnetic nanoparticles for magnetic resonance imaging (MRI). These systems have been applied *in vivo* for a variety of purposes, including preoperative imaging for tumour therapy, cancer tumour detection, visualization of tissues in pulmonary and heart diseases, imaging of inflamed areas and many others. The goal of this literature review is to assess the current state of BCP micelles in bioimaging including common techniques used in clinical practice, such as fluorescence imaging, positron emission tomography (PET), MRI and computerized tomography (CT).

Keywords: Block copolymer micelles, contrast agents, bioimaging, active targeting.

Table of Contents

..... 1
Abstract 2
Table of Abbreviations 4
Introduction 5
1. Block copolymer micelles 5
1.1 Categorization 5
1.2 Synthesis 6
1.3 Properties 7
1.3.1 High colloidal stability & Circulation Time 7
1.3.2 Chemical versatility 8
1.3.3 High loading capacity 8
1.3.4 Responsiveness to External and Endogenous Stimuli 9
2. Medical imaging 12
2.1 Radiology 13
2.1.1 Computed Tomography (CT) 13
2.1.2. Positron Emission Tomography (PET) 13
2.1.3 Magnetic Resonance Imaging (MRI) 14
2.2 Optical Bioimaging 19
3. Review: Polymer Micellar Nanostructures in Bioimaging 23
3.1 BCP Micelles in Optical Bioimaging 23
3.1.1 Polymeric Micelles & Conventional Probes 23
3.1.2 Polymeric Micelles & AIEgens 24
3.1.3 Polymeric Micelles & Quantum Dots 27
3.2 BCP Micelles in Magnetic Resonance Imaging 30
3.3 BCP Micelles in PET Imaging 40
3.4 BCP Micelles in CT Imaging 41
3.5 BCP Micelles in Multimodal Imaging 43
Conclusions & Future Perspectives 49
References 51

Table of Abbreviations

Table 1. Table of Abbreviations.

Abbreviation	Description
BCP	Block Copolymer
PICM	Polyion Complex Micelles
CMC	Critical Micellar Concentration
RES	Reticuloendothelial System
PEG	poly(ethylene glycol)
TME	Tumour Microenvironment
LCST	Lower Critical Solution Temperature
NIR	Near-infrared
PEG	Polyethylene Glycol
CT	Computed Tomography
PET	Positron Emission Tomography
SPECT	Single-photon Emission Computed Tomography
MRI	Magnetic Resonance Imaging
CA	Contrast Agent
SPIONs	Superparamagnetic Iron Oxide Nanoparticles
EPR	Enhanced Permeability and Retention
CEST	Chemical Exchange Saturation Transfer
NIR	Near Infrared
FDA	US Food and Drug Administration
EMA	European Medicines Agency
AIEgen	Aggregation-induced Emission Fluorogens
FRET	Förster Resonance Energy Transfer
QDs	Quantum Dots

1. Block copolymer micelles

1.1 Categorization

Block copolymer (BCP) micelles can be distinguished into three separate categories according to the nature of the supramolecular forces leading to their formation. [1]

a. Amphiphilic micelles (development of hydrophobic bonds between lipophilic blocks)
b. Polyion complex micelles, PICMs (self-assembly is driven by electrostatic interactions)
c. Micelles from metal complexation

Amphiphilic BCPs are macromolecular chains consisted of hydrophilic and hydrophilic blocks, and as a result they form micellar supramolecular nanostructures (5-100 nm) when suspended in a selective solvent. In the case of the solvent being water, the hydrophobic blocks aggregate spontaneously to form a collapsed core, surrounded by the hydrophilic chains forming a corona upon interaction with the surrounding aqueous environment (**Figure 1**). The resulting core-shell nanostructures are being immensely studied by the scientific community as drug carrier vehicles, since they are able to host hydrophobic pharmaceutical compounds in their core, while presenting excellent physicochemical and biological properties among other nanocarriers, such as liposomes, nanohydrogels and inorganic nanoparticles. [2]

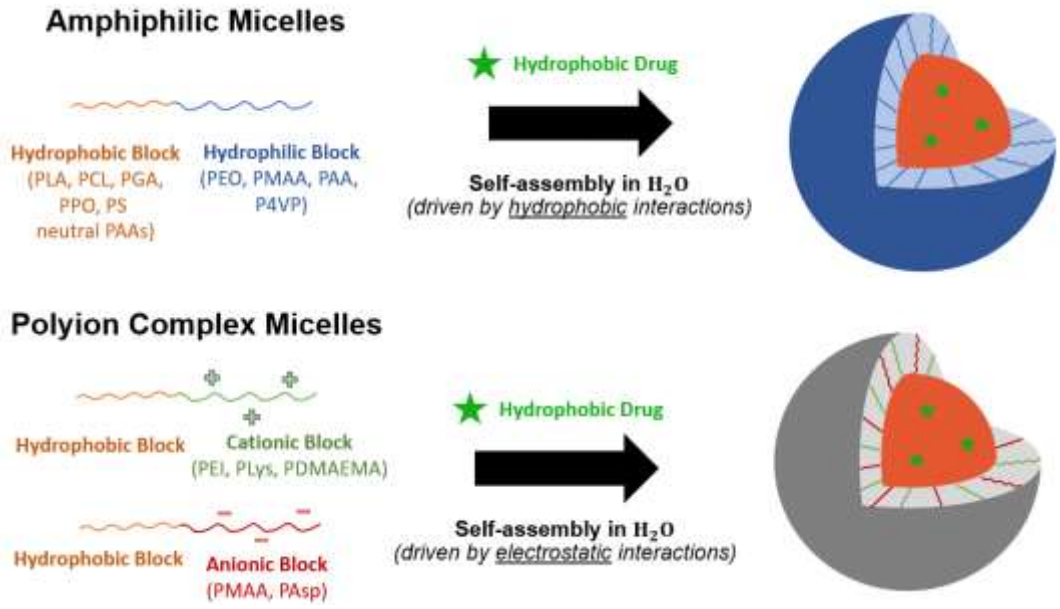

Figure 1. Schematic representation of amphiphilic and polyion-complex BCP micelles.

The final morphology of the micelles highly depends on synthetic parameters and the chosen ratio between the hydrophilic and the hydrophobic polymer blocks. Spherical morphology is usually observed when the hydrophilic block is longer than the hydrophilic one, while in the opposite case a lamellae morphology is favoured (polymersomes). [3]

During the recent years the conventional micellar assembly of a copolymer with a hydrophobic and a hydrophilic part, has been reconsidered. Exotic nanomicelles (referred as "schizophrenic" micelles, **Figure 2**) have been developed with interchanging hydrophobic and hydrophilic blocks depending on the presence of external stimuli (temperature, pH, ions). This process of "switching" is reversible and this type of systems are very promising for sensing applications. A notable example of this case is the development of poly(methacrylic acid-*block*-N-isopropyl acrylamide) switchable micelles with stimuli-responsiveness to calcium ions and heat. [4], [5]

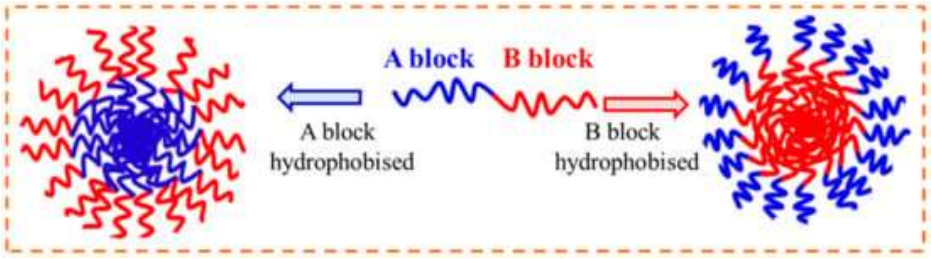

Figure 2. The concept of "schizophrenic" micelles with switchable hydrophobic and hydrophilic parts. **[5]**

1.2 Synthesis

The most common method for the preparation of BCP micelles is their direct dissolution of the polymer and the drug in aqueous medium (**Figure 3**). Upon dissolution, the formation of micelles via self-assembly is entropically prioritised to eliminate thermodynamically undesirable interactions between the hydrophobic segments and the surrounding water molecules. [6] The formation of micelles is experimentally facilitated by magnetic stirring, and usually heating or ultrasonication to obtain monodisperse nanoparticles. This method is ideal for water-soluble BCPs (poloxamers, PICMs). For the distinctive case of PICMs, BCP and the encapsulant are dissolved separately in aqueous media (deionized water or buffer solution), and then are combined for the formation of the micelles. [7]

Unlike direct dissolution, the dialysis method is suitable for amphiphilic BCPs with low aqueous solubility. In this case, the polymer and the encapsulant are both dissolved in a common organic solvent (e.g., N-N,dimethylformamide or dimethylsulfoxide). Micellization is induced by the addition of water in the system, and the suspension is further dialysed in water to slowly remove any trace of organic solvent. [7]

Alternatively, the BCP and the drug can be dissolved in a common organic solvent, and upon solvent evaporation, the micelles can be formed by hydrating the resulting

film with water (solvent evaporation). To achieve a micelle suspension with low polydispersity, the redispersed particles should be sonicated. Otherwise, the polymer and the encapsulant can be dissolved in an organic cosolvent followed by the addition of water to the system (cosolvent evaporation). After the evaporation of the cosolvent the suspension of the micelles will be formed in the aqueous phase. Lastly, BCP micelles can be prepared by freeze-drying the mixture of polymer and drug in water/tert-butanol (high vapor pressure) and redispersing the solid in an aqueous solution. [6], [7]

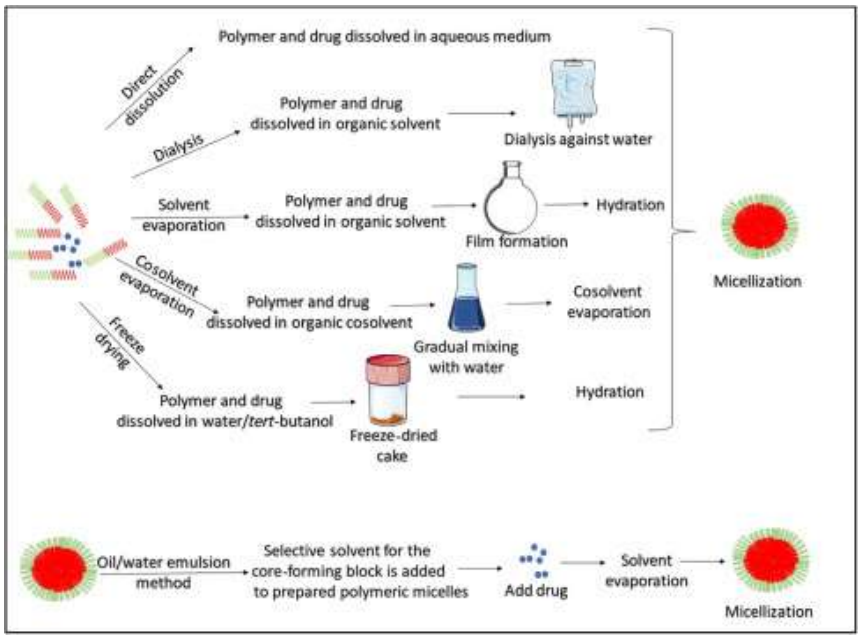

Figure 3. Preparation methods for BCP micelle synthesis. **[6]**

1.3 Properties

1.3.1 High colloidal stability & Circulation Time

One of the most advantageous properties of BCP micelles is their enhanced colloidal stability compared to the chemical class of surfactants that are also used for the solubilization of hydrophobic pharmaceutical compounds. This property stems from their ultra-low critical micellar concentration (CMC), above which the formation of micellar structures is favoured. [8] For most BCP micelles CMC fluctuates between $10^{-6} - 10^{-7}$ M, while for commercial surfactants CMC is quite higher ($10^{-3} - 10^{-4}$M). [6]

The hydrophilic shell of BCP micelles has a dual role; the steric repulsions afforded by the polymeric chains facilitates the colloidal stability of the system in high ionic strength media, while their uptake by reticuloendothelial system (RES) is delayed resulting in increased circulation time. The most commonly used hydrophilic block is poly(ethylene

glycol) (PEG), known for its high biocompatibility and ability to not evoke unwanted responses from the immune system (stealth nanosystems). [9]

1.3.2 Chemical versatility

BCP micelles exhibit great chemical versatility since they can obtain different morphology depending on the synthetic parameters chosen, and as a result the nature of the intermolecular forces formed. Apart from the typical hydrophobic core-hydrophilic shell micelles described above, reverse micelles can be obtained in non-aqueous media, as presented in **Figure 4**. In addition, by using a triblock copolymer (A-B-A type) multi-compartment micelles can be synthesized for the simultaneous release of pharmaceuticals entrapped in the different nano-compartments. Alternatively, multi-compartment micelles can be formed by covalently grafting a third polymer onto the copolymer backbone (A-B-C type). Finally, stimuli responsive moieties can be introduced in the polymer blocks to fabricate sensitive micelles for intracellular drug release and biological targeting applications, that will be further described below. [3]

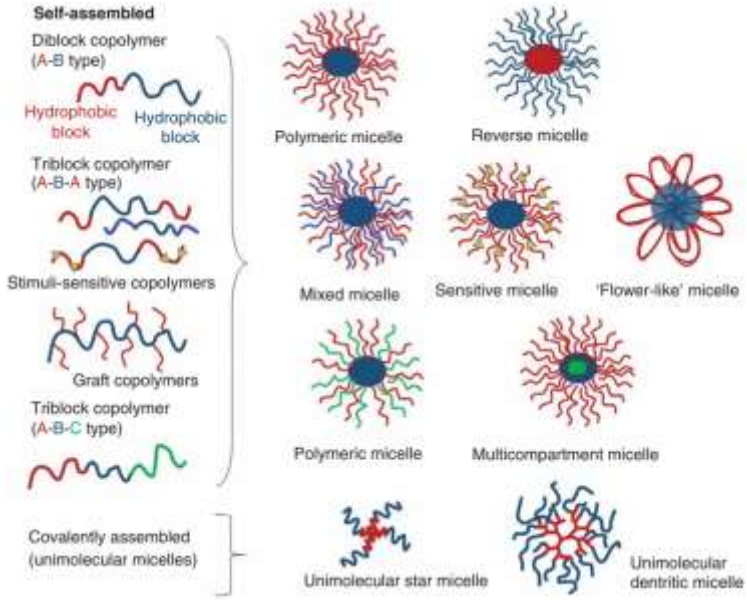

Figure 4. Different types of BCP micelles based on the nature of intermolecular forces involved. [3]

1.3.3 High loading capacity

As mentioned above, hydrophobic interactions are the driving force for the encapsulation of lipophilic drugs into the micelles' cores. However, by appropriately selecting the hydrophobic polymer, the encapsulant can be covalently attached to the core. For instance, poly-(α,β-aspartic acid) has been used for the covalent conjugation of doxorubicin in PEG-PAsp BCP micelles via a condensation reaction between the

lateral carboxylic groups of the polymer and the amine group of doxorubicin. [8] Covalent encapsulation offers the advantages of higher drug loading and lower rate of encapsulant leakage from the micelles. [10]

1.3.4 Responsiveness to External and Endogenous Stimuli

Block copolymer micelles are excellent candidates for building stimuli-responsive vehicles of contrast agents. Site-specific stimuli can be categorized to exogenous (temperature, light, magnetic/electric field, ultrasound) and endogenous (pH, enzymes, redox environment, presence of ions or other biomolecules). [11]

Temperature

BCP micelles present their chains expanded in the aqueous environment, and thus they are stable in colloidal suspension when the temperature of the solution is under the lower critical solution temperature (LCST). Above LCST, the hydrogen bonds between the water molecules and the hydrophilic polymeric block are cleaved (dehydration). As a result, the micelle suspension is destabilized, and the particles precipitate form the solution. According to **Figure 5**, polymers such as poly(*N*-isopropylacrylamide) (PNIPAAm) and PEG-PPO-PEG, also knows as Pluronics, are widely used for the development of thermoresponsive micelles. [12]

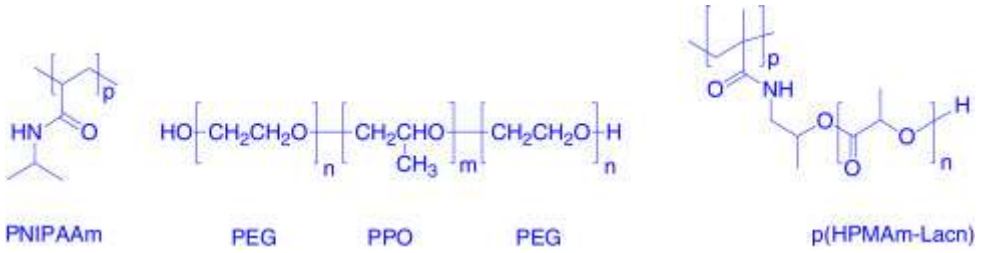

Figure 5. Polymer structures that are used for the fabrication of thermoresponsive BCP micelles. **[12]**

An interesting application of this property is photothermal therapy for cancer treatment, where temperatures above 43℃ are achieved inside the TME. Poly(ε-caprolactone)-block-poly(N-isopropylacrylamide-co-N,N -dimethylacrylamide) (PCL- b-P(NIPAM-co-DMA) micelles have been used as a thermoresponsive platform for cancer photothermal therapy. By adjusting the polymer components' molar ratio in the final formulation, LCST was tuned at 42℃ to achieve responsiveness to cancer hyperthermia. A photothermal dye (indocyanine green) was loaded into the micelles and via excitation with near-infrared (NIR) light, intracellular delivery of the loaded chemotherapeutic agent (doxorubicin) was achieved. [13]

Light

Light (UV, visible or NIR) is an interesting case of external stimuli, since it can be easily applied and controlled (in terms of wavelength and intensity) outside of the biological environment. Light-responsive BCP micelles can be classified into two distinct categories based on the mechanism of disruption, systems with light-switchable properties (e.g., polarity change due to photoisomerization) and micelles that exhibit light-induced bond cleavage upon irradiation. The most common modification for the fabrication of light-responsive BCP micelles is the addition of azobenzene photochromic groups which reversibly isomerize (cis-trans) in the presence of UV-visible light. [14] In the case of light-induced bond cleavage, micelles with covalently attached chemotherapeutic agents have been developed. For instance, doxorubicin, a widely used chemotherapeutic agent, can be covalently conjugated to polyethylene glycol (PEG) chains via a UV-sensitive amide bond. In this fashion intratumoral release of doxorubicin upon exposure to UV light was achieved, avoiding the occurrence of unwanted side-effects during osteosarcoma treatment. [15] A more recent and effective approach is the activation of the micelles with the use of NIR light (650-900 nm), which is safer to UV radiation and allows deep-tissue penetration due to less scattering from the biological tissues. In this manner, NIR-responsive shell-crosslinked micelles have been synthesized for the co-encapsulation of doxorubicin and indocyanine green. The NIR-responsiveness is attributed to the diselenide bonds offered by the cross-linker (bis(maleimidoethyl) 3,3′-diselanediyldipropionoate) via a Diels-Alder reaction. Upon NIR-irradiation the micelles' coronas disintegrated and controlled drug release was achieved inside the TME. [16]

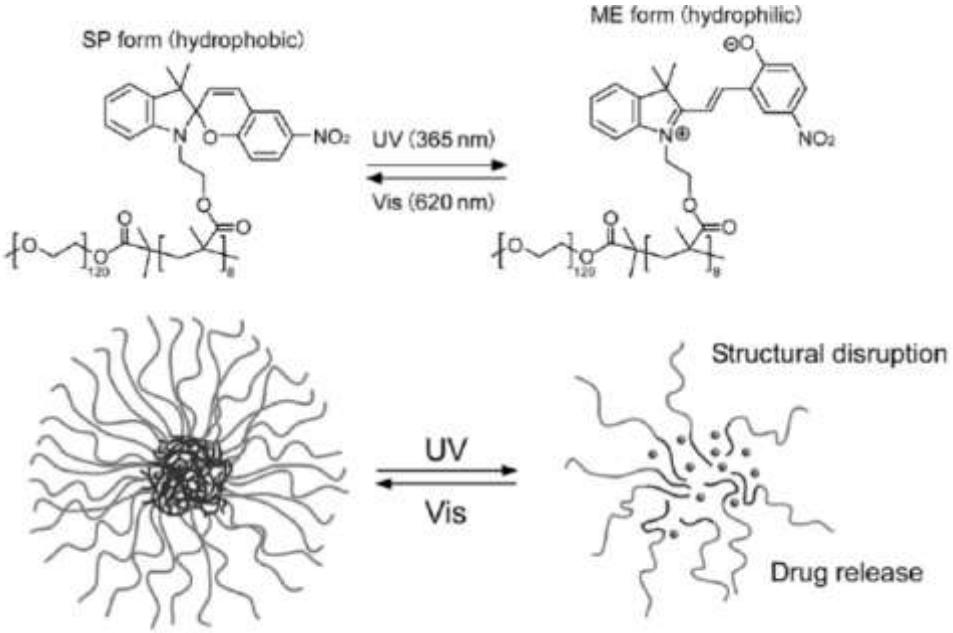

Figure 6. An example of light-responsive BCP micelles bearing a photo-switchable spiropyran moiety. **[14]**

pH

Responsiveness to the pH of a solution can be achieved by choosing polymer blocks with acidic or basic lateral groups, as shown in **Figure 7**. Fluctuation of pH can potentially change the protonation state of these groups, and as a result modify the polymer's configuration, as well as the micelle's overall morphology and properties. [5] This property is really beneficial for building drug delivery systems with responsiveness to the characteristics of the environment of the biological target. Thus, the loaded cargo is released selectively to the derisible tissue, avoiding the accumulation in the nearby healthy cells that usually leads to side-effects. The tumour microenvironment (TME) is a great example, since it presents slightly acidic pH (6.5-7.2) compared to the extracellular environment of healthy tissues (pH=7.4). This is attributed to the hypoxic state of the TME and the overproduction of lactic acid by the tumour cells. Another example is the acidic pH of endosomes (5.0-6.0) and lysosomes (4.0-5.0) during the cellular internalization of a drug delivery system. Borth pH gradients can be used to develop sensitive micelles that are stable in the physiological pH, but they can disintegrate in the presence of acidic pH and as a result release their cargo in the TME and/or in the subcellular organelles during endocytosis. [17]

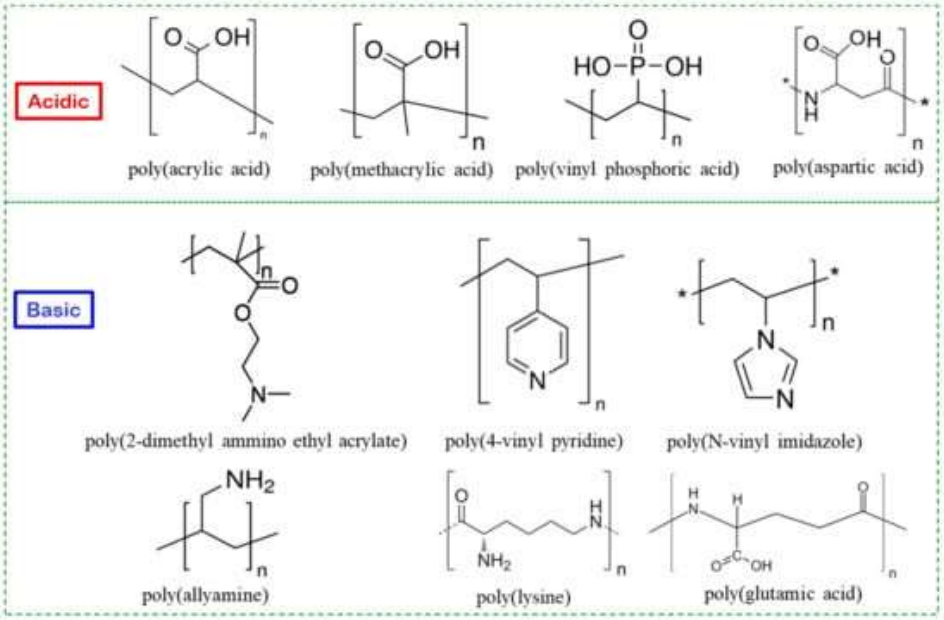

Figure 7. pH-responsive building blocks for BCP micelles**. [5]**

Redox responsiveness

One of the most interesting endogenous stimuli to look for during the design of highly selective contrast agents, is the reducing habitat of certain biological sites, such as the TME. BCP micelles can be chemically modified to host redox-responsive moieties, such as disulfide and diselenide bonds. The elevated concentration of glutathione inside the tumour cells compared to the nearby healthy tissue, leads to the reduction

of sulphur and selenium, and eventually the cleavage of the respective bonds. Thus, micelles comprised of redox-responsive polymers are able to release their cargo inside the biological target with high specificity, avoiding premature leakage in the surrounding tissue. In more detail, disulfide bonds can be introduced to the micellar structure as cross-linking agents for the core or the shell. For instance, triblock PEG-b-PLys-b-Ppha micelles have been used for the introduction of a disulfide crosslinker in the middle compartment, to achieve enhanced stability and prolonged release of the encapsulant. Alternatively, a crosslinking moiety can be introduced to the core of the micellar structure, as it has been achieved with PEO-b-PFMA micelles via Diels-Alder reaction, for the site-specific release of doxorubicin (**Figure 8**). [18]

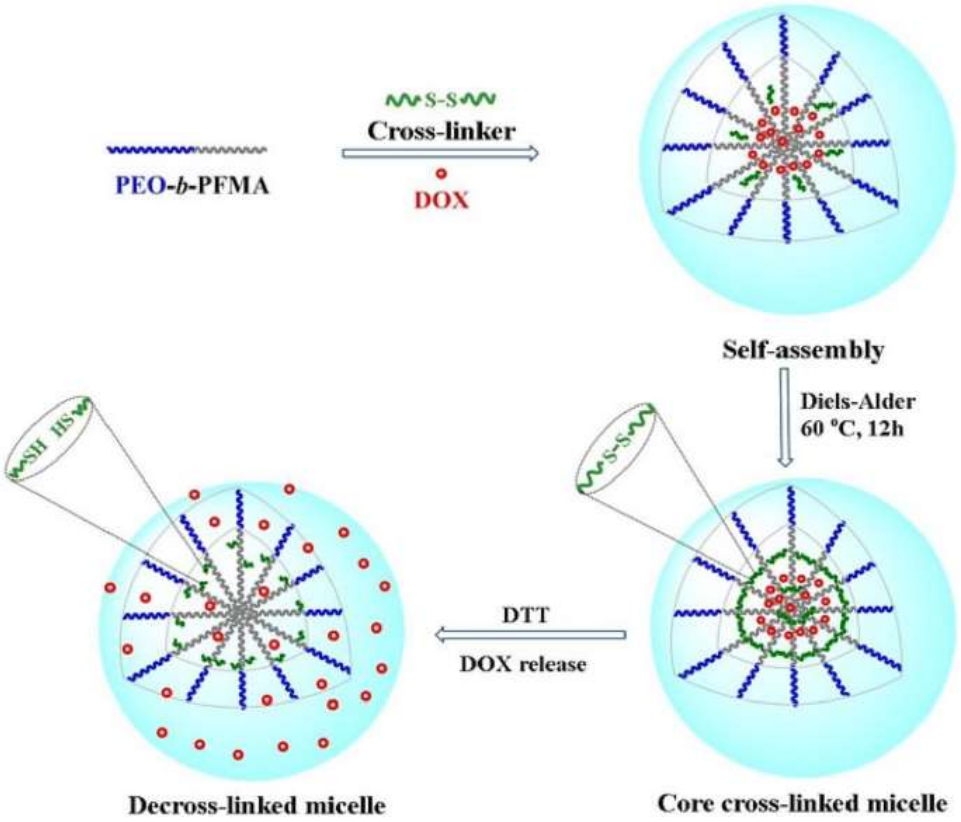

Figure 8. Redox-responsive core-crosslinked micelles based on the cleavage of the disulfide bonds in the TME. **[18]**

2. Medical imaging

According to ImageCLEF 2015, medical imaging modalities can be categorized in five distinctive groups depending on the nature of the image output: [19]

a) Radiology
b) Visible Light Photography
c) Printed Signal (Waves)
d) Microscopy

e) 3D Reconstruction

For the purposes of this study, the focus will be held on Radiology and Microscopy techniques, where BCP micelles exhibit the most interesting applications.

2.1 Radiology

In the branches of diagnostic and interventional radiology, several imaging techniques are included, such as X-ray imaging, Computed Tomography (CT), Positron Emission Tomography (PET), Single-Photon Emission Computed Tomography (SPECT) and Magnetic Resonance Imaging (MRI). The main purpose of the aforementioned techniques is to visualize the anatomy and the abnormalities of biological tissues, as a mean of diagnosis for a variety of diseases, including cancer, cardiovascular diseases and neurological disorders. [20]

2.1.1 Computed Tomography (CT)

Computed Tomography (CT) is a medical imaging method that utilizes X-rays to obtain images from almost every part of the human body, ranging from soft tissues and bones to the brain, the heart and blood vessels. CT is based on X-ray attenuation by high-atomic number elements that absorb X-ray photons via the photoelectric and the Compton effects. The X-ray attenuation μ_x is quantitively expressed in Hounsfield Units, as calculated by the Equation 1.

$$\text{Attenuation (HU)} = 1000 \cdot \frac{\mu_x - \mu_{water}}{\mu_{water} - \mu_{air}} \quad (1)$$

where μ_{water} is the attenuation of water (0 HU) and μ_{air} the attenuation of air (-1000 HU).

In clinical practice iodinated contrast agents have been approved (Iohexol). Novel contrast agents based on nanomaterials have been recently developed, with higher circulation half-time and sensitivity. Despite its widespread use, CT presents limitations compared to other imaging techniques (e.g., MRI), such as low sensitivity to contrast and exposure to ionizing radiation. [21]

2.1.2. Positron Emission Tomography (PET)

Positron Emission Tomography (PET) is a widely used imaging modality well-known for its ultra-high sensitivity and ability for quantification among different imaging techniques. PET provides physiological information based on the photon emission of radioisotopes, which are injected into the patient. The produced positron from the radioactive decay of a radiotracer, such as F-18, interacts with an electron in short

distance, and as a result photons are emitted due to the positron-electron annihilation. The emitted photons are detected by the PET scanner that uses scintillation crystals and photomultipliers. [22]

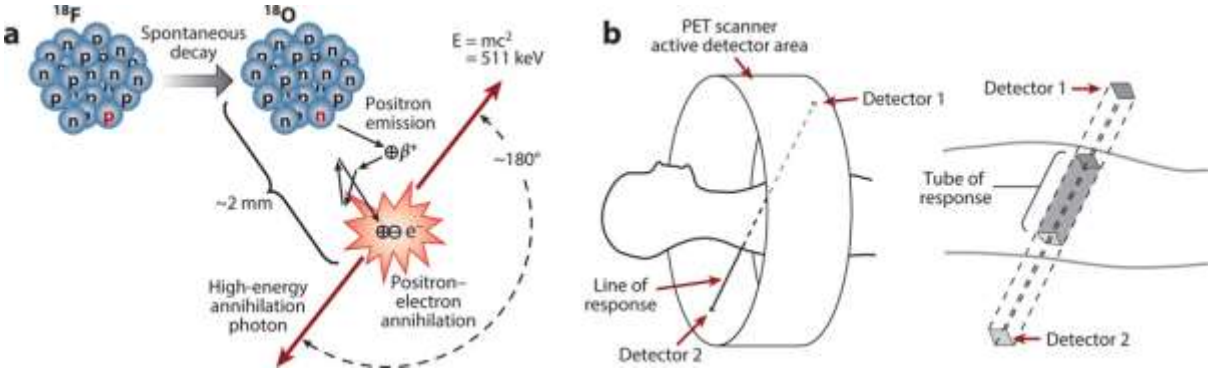

Figure 9. a) Example of the radioactive decay of F-18 in PET imaging and the underlying mechanism. b) Position of the patient **[22]**

The novel properties of nanoscale (ultra-high surface area, chemical versatility, biological targeting) have introduced various nanomaterials in the field of PET imaging. The main advantages of nanomaterials over conventional traces, can be classified as following: [23]

1. Signal amplification (high contrast).
2. Functionalisation with targeting moieties.
3. Imaging multimodality (e.g. radiolabelled iron oxide NPs for dual PET/MRI).
4. Combination of therapeutic and diagnostic modalities (theranostics).

2.1.3 Magnetic Resonance Imaging (MRI)

Unlike the previous imaging methods, Magnetic Resonance Imaging (MRI) does not operate with radiation but with the inherent magnetic properties of the human body. It is known that the majority of human tissue is comprised of water, and thus proton nuclei that exhibit magnetic angular momentum (spin). Given that each proton in the human body acts as a microscopic magnetic rod, when there is no external magnetic field the magnetic vector of each proton will be randomly oriented to every direction. In this case, the sum of the magnetic vectors will be calculated as zero. However, when a potent magnetic field is applied (1.5 or 3.0 Tesla), all the protons will interact with it and start rotating with a specific frequency, abandoning their random state that they had before. After the excitation finishes, all the nuclei return to their ground state by emitting the energy difference as electromagnetic radiation (relaxation). During the relaxation process the longitudinal and the transverse vertices of the total magnetic vector, which are independent from each other, return to the original equilibrium

values. Transverse magnetization can return back to zero quite faster than the longitudinal one.

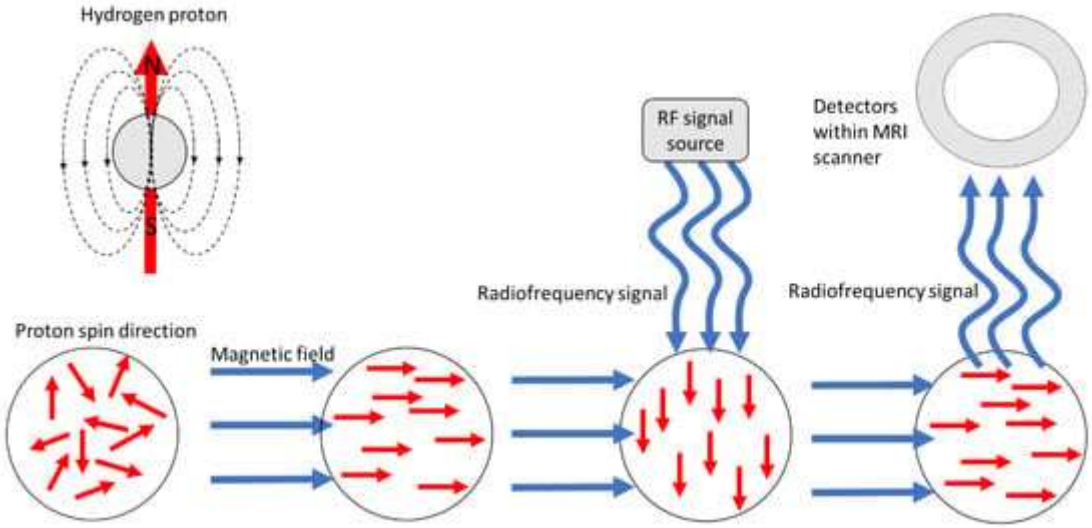

Figure 10. Schematic representation of the MRI signal acquisition mechanism. **[24]**

The relaxation process is described by two important parameters, T1 and T2. T1 (spin-lattice relaxation time) is the time required for the nuclei to reach 63% of their original longitudinal magnetization. In other words, T1 expresses the speed in which the energy is dispersed back to the molecular environment of the excited nuclei. On the other hand, T2 is defined as the time period required for the transversal magnetization to reach the 37% of its initial value. It expresses the speed in which the transverse magnetization attenuates and returns back to the ground state.

T1 and T2 values present unique values for each biological tissue and they depend on the amount of the “free” water molecules that are present in the biological environment. T1 enhances the signal of the fatty tissue and supresses signal from water. T2 enhances signal of water molecules.

The brightness of the final MRI image is dependent on the intensity of the signal (higher intensity leads to brighter areas, while lower signal appears as darker grey). Areas with high intensity are described by the following features:

i) Low T1 value
ii) High T2 value
iii) High proton density

In order to reduce the spin-lattice relaxation (T1) value, the following strategies can be followed: [25]

a) Reduction of the tumbling rate (movement) of the surrounding molecules. This can be achieved with the presence of high-weight compounds (fat, lipids, glycoproteins etc) or by decreasing the tissue temperature. The latter is usually applied in post-mortem examinations.

b) Binding of the protons, which can be achieved by using paramagnetic contrast agents to increase the proton precession frequency.

So, besides the intrinsic contrast of the biological tissues, contrast agents (CA) have been introduced in medicine to provide MRI anatomical visualization of higher quality. The sensitivity of a contrast agent is expressed by its relaxivity (r_i) according to Equation (2).

$$\frac{1}{\mathrm{T_i}} = \frac{1}{\mathrm{T_i^0}} + \mathrm{r_i} \cdot [\mathrm{CA}], \mathrm{i} = 1, 2 \quad (2)$$

where $[\mathrm{CA}]$ stands for the contrast agent's concentration and $\mathrm{T_i^0}$ for the relaxation time of the tissues in absence of the contrast agent. By choosing a contrast agent with high relaxivity, higher contrast can be achieved by administrating lower dosage and as a result avoiding the occurrence of side-effects at the same time. [26]

MRI CAs can be categorized regarding their magnetic properties into two major groups:

1) Paramagnetic CAs, usually consisting of transition and lanthanide metal complexes (Gd^{3+}, Dy^{3+}, Mn^{2+})
2) Superparamagnetic CAs (superparamagnetic iron oxide nanoparticles)

Paramagnetic CAs possess unpaired electrons in their valance layer, and as a result they modify the relaxivity of the neighbouring protons present in the water molecules of biological tissues (Figure 11A). The contribution of the CA to the water magnetization depends on their molecular distance. Inner-sphere relaxation stems from the water molecules that are conjugated on the paramagnetic center, while the outer-sphere relaxation is attributed to the bulk water molecules present in larger distance. [27] The most widely used paramagnetic CAs are based on gadolinium, which reduces the T1 and T2 relaxation times of the neighbouring protons. Thus, the contrast of T1-weighted MR images is enhanced, while the signal of the T2-weighted ones is reduced. A variety of CAs based on the chelating complexes of the stable gadolinium ions have been approved by FDA and are used in clinical practice, with more than 100 million patients having undergone Gd-based MRI over the past 25 years. [28], [29] In this particular case, gadolinium is usually chelated with organic compounds to increase the biocompatibility of the CA and eliminate the appearance of side-effects in clinical MRI. Thus, the water molecules coordinate to the organic chelator, instead of the gadolinium ion itself, and as a result forming the second sphere as depicted in Figure 11B. It is apparent that the surface chemistry of a CA has a critical role in its efficiency in the clinical practice. Surface ligands that facilitate the rapid exchange of water molecules lead to CAs with higher T1 relaxivity (Figure 11C), while coating the surface of a CA with another material leads to higher T2 relaxivity but lower T1 potency (Figure 11D). [27]

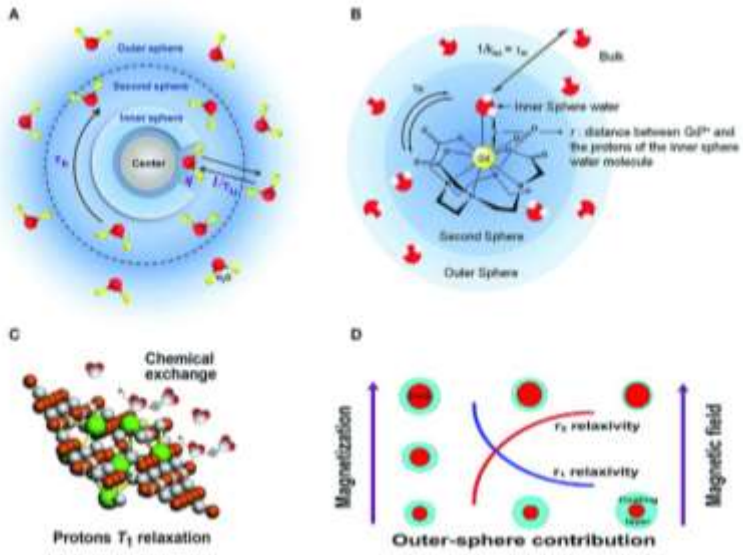

Figure 11. a) Schematic representation of the change in proton magnetization offered by a paramagnetic contrast agent in aqueous environment. b) Coordination of water molecules to the organic chelator of a gadolinium-based CA. c) Chemical exchange of water molecules from surface ligand facilitates T1 relaxation. d) Effect of surface coating of a CA to its T1 and T2 relaxivities. **[27]**

Superparamagnetic CAs, such as iron oxide and superparamagnetic iron oxide nanoparticles (SPIONs), are used in T2-weight MRI providing dark contrast. Initially, SPIONs were applied in diagnostic imaging for liver cancers, since they presented increased uptake by liver macrophages (Kupffer cells). This property is attributed to the ability of SPIONs to be captured by the RES. However, due to the relatively large size (around 50 nm) they did not show significant accumulation in solid tumours through the EPR effect, since they were rapidly excreted by macrophages. New-generation SPIONs were designed to show large circulation times and increased accumulation in solid tumours through the EPR effect. Their ultrasmall size of around 6 nm and their dextran coating affords a final formulation with a circulation time greater than14 h in the human body. SPIONs are commercially available for MRI, with various brand names including Feridex, Resovist and Ferumoxytol. Certain advantages of SPIONs, such as the fact that iron occurs naturally in the human body in contrast to gadolinium, bring this type of CA in the forefront of MRI. Figure 12 depicts the different impressions of gadolinium-based CAs and SPIONs in T1- and T2-weigthed images. [29]

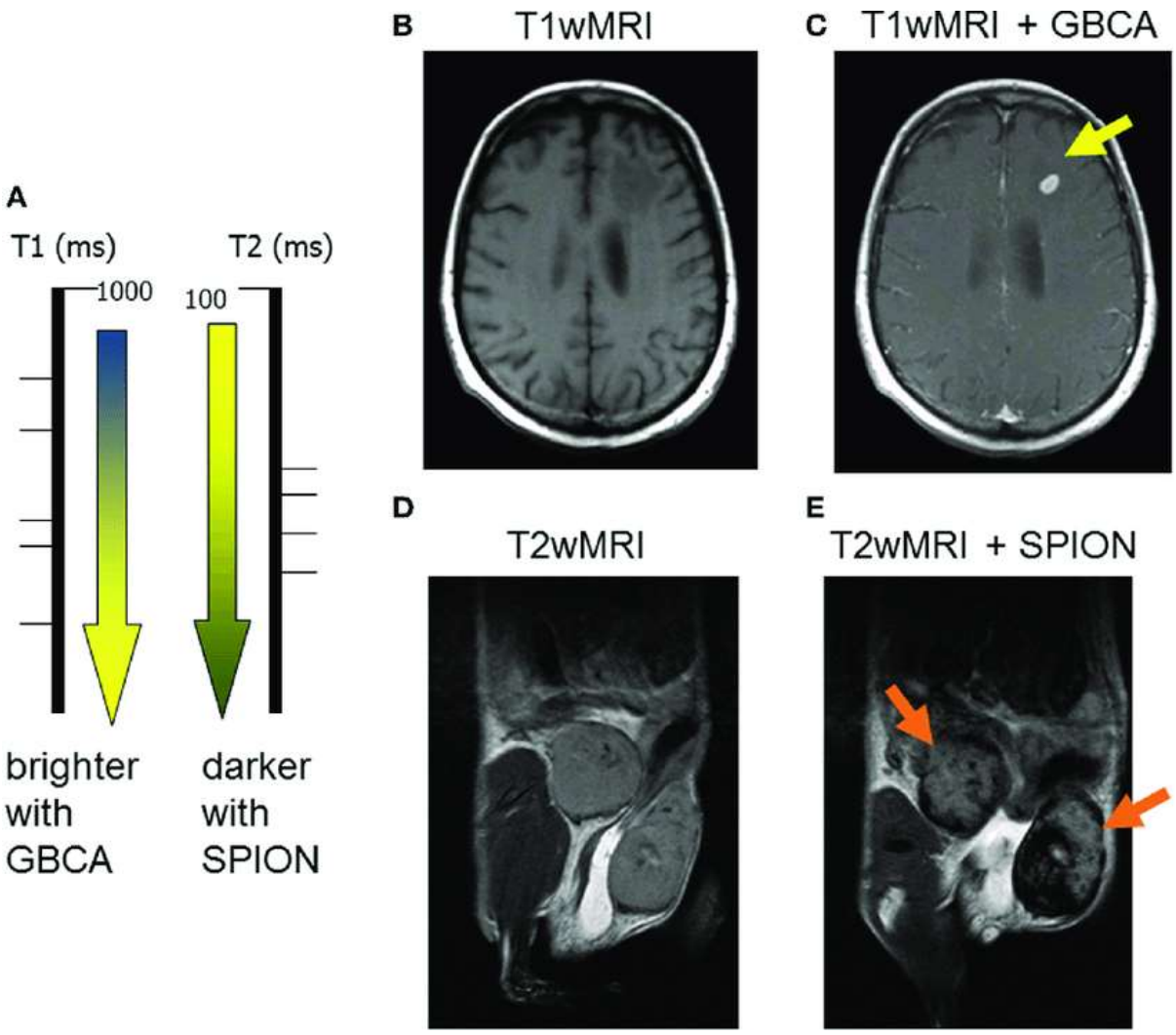

Figure 12. A) The 2 major groups of CAs in MRI: the Gadolinium-based CAs that reduce the T1 relaxation time of the surrounding molecules affording brighter contrast, and the SPIONs that are T2-shortening agents leading to darker contrast in the final image. B) Before- and C) 15 mins after the injection of a gadolinium-based CA in a patient with metastasized melanoma in the brain (the tumour is detected in the bright area as observed in the T1-weighted MRI). D) Before- and E) 24h after the injection of SPIONs in mice with inflamed mammary gland tumours (the tumour site appears darker in the T2-weighted image due to the accumulation of SPIONs). **[29]**

To increase the sensitivity of MRI other magnetic nuclei can be used except ^{1}H, such as ^{13}C, ^{15}N, ^{19}F, ^{31}P and ^{129}Xe. This way the intrinsic contrast of human tissues can be eliminated and achieve higher MRI signals. Also, metabolic pathways can be thoroughly investigated by MRI, in a large variety of applications including the nervous system, heart and pulmonary diseases, cancer tumours, stroke, inflammation and others. [30]

Another emerging category of MRI CAs is based on Chemical Exchange Saturation Transfer (CEST). Unlike conventional ^{1}H MRI, CEST is based on exchangeable protons that are moving back and forth between the contrast agent and the surrounding water molecules. Thus, when applying radiofrequencies the following MRI

attenuation is transferred from the CEST CA to the water molecules nearby, since the magnetic modulated protons are able to relocate. As a result, MRI signal is created (**Figure 13**). Candidates for CEST imaging are small molecules, polymers and nanoparticle systems (carbon dots, liposomes, dendritic polymers) that bear functional groups that are capable of proton exchange in the aqueous environment. Regarding polymers, polyaminoamine (PAMAM), poly-L-lysine (PLL), poly-acrylic acid (PAA) and dextrans have been used for the fabrication of hybrid CEST-traceable nanosystems. [31]

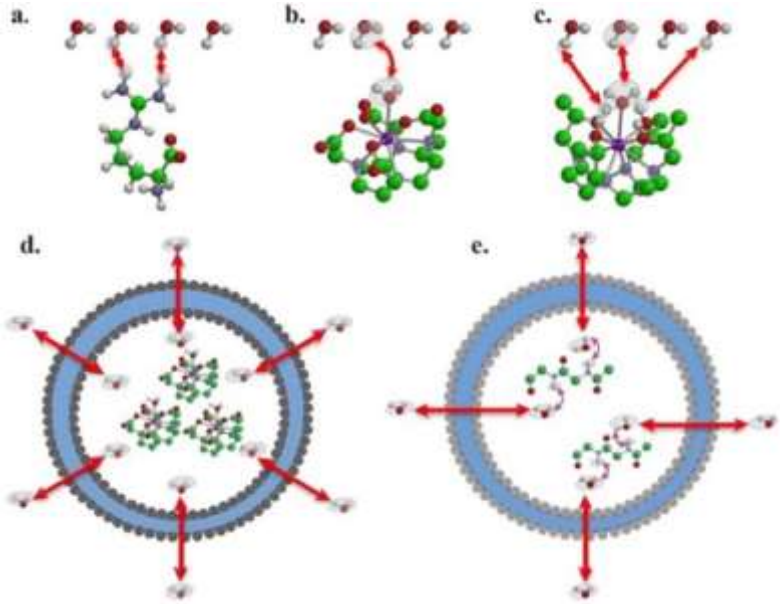

Figure 13. Different mechanisms of action of CEST MRI CAs. a) $^{+}$H transfer, b) molecule transfer, c) molecule and $^{+}$H transfer, d) change of compartment, e) molecule-mediated change of compartment. **[31]**

2.2 Optical Bioimaging

Optical techniques are less invasive alternatives in medical imaging and they have received increasing attention the recent years by the scientific community. In every case, optical imaging is based on the interactions occurring between light and biological tissues, that reflect photochemical changes on a molecular level, such as photon absorption and fluorescence. This category of techniques can be divided into microscopy-assisted methods, such as confocal microscopy for studying biomarkers in cellular and subcellular levels, and macroscopic imaging of biological sites for preoperative guidance in surgical applications. In particular, fluorescence imaging has been widely investigated in clinical practice by using molecular fluorescent tags, which include fluorescence proteins, dyes, other organic probes and nanomaterials. [32]

Fluorophores stimulated by longer wavelength radiation, especially in the red visible and near-infrared (NIR) regions of the spectrum, are suitable for the imaging of tumours in areas of the body with limited accessibility (e.g. intracranial tumours). Red

light has a higher permeability to biological tissues and rarely causes photosensitivity to the skin (Figure 14). At lower wavelengths (<600 nm) there is increased scattering of radiation by biological tissues, due to radiation absorption by tissue chromophores (melanin, haemoglobin), ultimately leading to lower absorption of the beam by the contrast agent. Therefore, the spectral region described by the 760-900 nm range is the optical "window" that allows maximum light penetration into biological tissues and the achievement of high signal-to-noise ratio (NIR-I). Inaccessible malignant tumours, such as glioblastoma, can be reached by using near infrared activated fluorescent probes that exhibit deeper tissue penetration in comparison to ultraviolet and visible light. Recently, the NIR-II and NIR-III (1000-1700 nm) optical windows have also been explored in fluorescence imaging to minimize background noise and maximise sensitivity. [33]

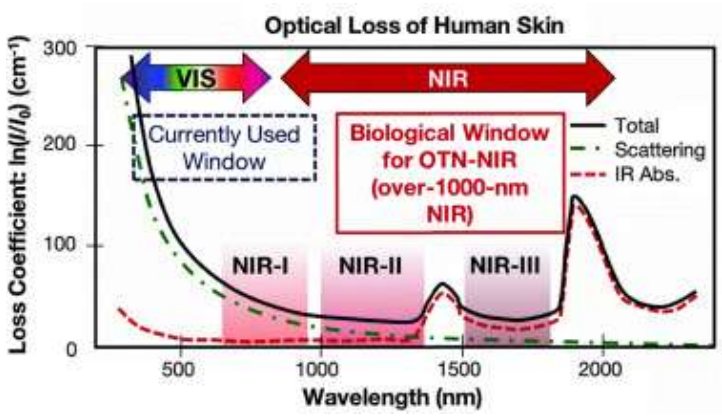

Figure 14. Light absorption spectrum of human skin. **[33]**

In clinical practice, NIR-fluorescence imaging has been applied with great results in real-time preoperative visualization of tumours, given that the fluorescence of the background is minimized in the NIR optical window. Thus, the fluorescence signal emitted by the probe inside the TME results to sharp contrast and can reach up to 10 mm in penetration depth to human tissues. A typical apparatus includes a NIR light source, a NIR-activated fluorescent probe that is intravenously administrated to the patient, and a camera that detects the emitted NIR light (Figure 15). The probes can be organic molecules with no biological specificity or fluorescent tags that are conjugated to a particulate system with active targeting characteristics. In the first category, FDA and EMA have approved the clinical use of three fluorophores, indocyanine green, methylene blue and 5-aminolevulinic acid. [34]

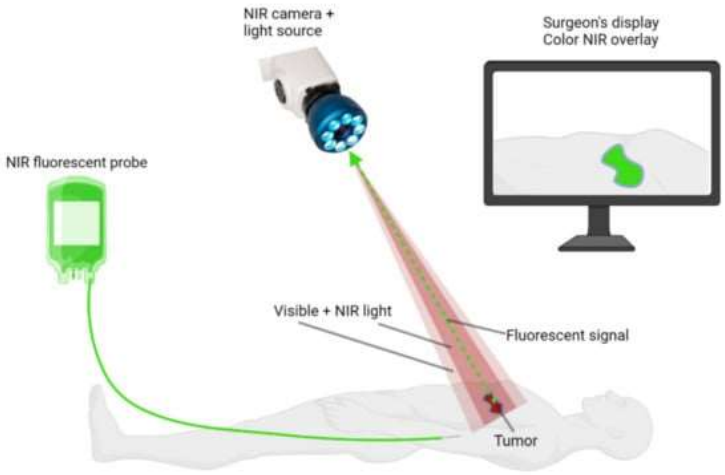

Figure 15. Typical apparatus for NIR-fluorescence imaging in preoperative and/or intraoperative visualization of the biological site of interest. **[34]**

Aggregation-induced fluorogens (AIEgens) are a new generation of fluorescent probes that present stable and enhanced emission (10-40 higher than conventional probes), when they form aggregates in solution. However, their monomer form is non-emissive, due to the restriction of their intramolecular rotation in aggregated state (Figure 16). Due to the rotor structure of AIEgens, they have the ability to rotate and vibrate freely in monomer state and as a result emit the absorbed energy via a non-radiative pathway. This phenomenon is reversed when these molecules aggregate and their degrees of freedom decrease significantly, affording chemical species with intense fluorescence. Unlike, conventional fluorescent probes, AIEgens present increased emission in their aggregated form bring a solution to a main drawback presented in the development of stable contrast agents. The aggregates can emit fluorescence in the visible spectrum, as well as in the NIR optical window, affording deeper tissue penetration and 3D images of high quality. Also, AIEgens can be used in two-photon fluorescence imaging for image-guided surgeries, since they have the ability to be excited in higher wavelengths. [35]

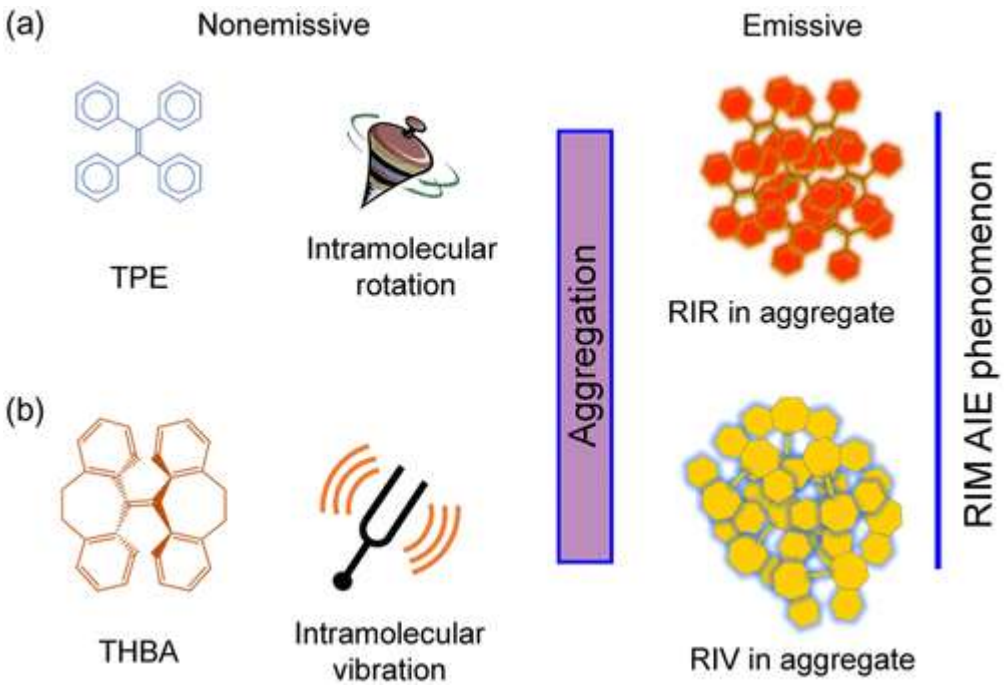

Figure 16. a) Restriction of the intermolecular rotation (RIR) of an AIEgen, such as tetraphenylethene (TPE), which results in aggregates with intense fluorescence emission. b) Restriction of the intermolecular vibration (RIV) of molecules such as THBA, for the generation of highly emissive aggregates. **[35]**

3. Review: Polymer Micellar Nanostructures in Bioimaging

3.1 BCP Micelles in Optical Bioimaging

3.1.1 Polymeric Micelles & Conventional Probes

FDA approved fluorescent probes, such as indocyanine green, present the inherent disadvantage of photobleaching and degradation upon irradiation. By encapsulating such fluorophores into the core of BCP micelles the above drawback is mitigated, resulting in highly stable fluorescent nanoparticles with long circulation times. A simple BCP such as PEG-PCL, has been used for this purpose, where the dye is incorporated inside the micelle's core via non-covalently hydrophobic interactions. Also given that indocyanine green can be excited (785 nm) and emit fluorescence (800 nm) in the NIR-I optical window, the described system can be used for NIR fluorescence imaging. To further increase the dye's photostability, a second fluorophore (IR-1061) can be co-encapsulated into the micelle's core and act as an acceptor chromophore in a process named Förster Resonance Energy Transfer (FRET). Specifically, indocyanine green is transferring its excess energy to the adjacent dye via dipole coupling, and as a result its excitation lifetime is decreased. This way, the probe in question is going to be decomposed in a lower rate upon irradiation. Considering the above, the final nanosystem presented excellent results for *in vivo* NIR fluorescence bioimaging in mice, visualizing their blood vessels and internal organs (Figure 17). It is worth noting that the nanomicelles remained stable for over 30 minutes in the blood circulation, emitting strong fluorescence in the NIR area. After that period, the nanoparticles started to accumulate in the liver and the spleen of the mice (due to RES capturing), as shown by the NIR imaging. In addition, the formulation presented enhanced toxicity to breast cancer cells upon irradiation, due to the dye's parallel photodynamic action, rendering the micelles an excellent candidate for cancer therapy and imaging. [36]

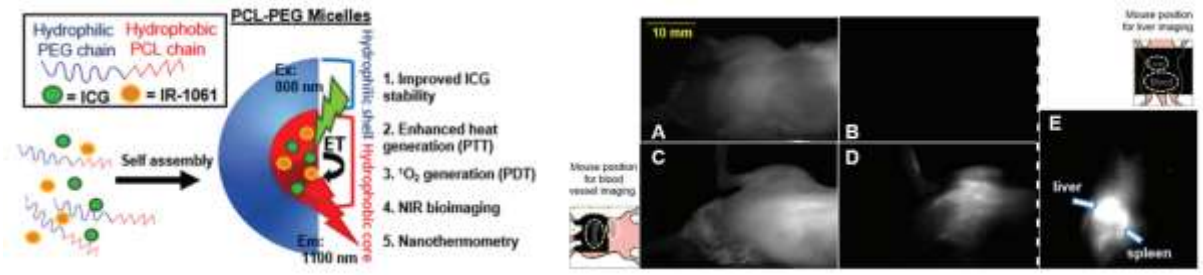

Figure 17. 1) Schematic illustration of the incorporation of indocyanine green and IR-1061 in PEG-PCL BCP micelles. 2) NIR fluorescence imaging *in vivo* with mice. A: visible light, untreated mice, B: NIR light, untreated mice, C: visible light, treated mice with micelles, D: NIR light, treated mice with micelles, E: NIR image 60 min after the micelle injection. **[36]**

3.1.2 Polymeric Micelles & AIEgens

Unlike the passive incorporation of conventional fluorescent probes, AIEgens are usually covalently conjugated with the micelles. Due to their hydrophobic nature, they can be grafted onto hydrophilic polymers and yield amphiphilic structures with the capability of micelle formation. Polysaccharides are a perfect example of natural hydrophilic polymers that can be chemically modified to afford micelles in solution. For instance, chitosan's polymeric backbone can be modified with TPE via an isothiocyanate-amino reaction, as presented in Figure 18, to yield highly emissive and photostable polymer conjugates due to the imposed intermolecular restriction. Unlike conventional dyes conjugated with polymers, AIEgen-modified structures present an augmentation in their fluorescence emission as the grafting density increases. The developed material has shown excellent properties for cancer cell staining and differentiation from healthy cell lines *in vitro*. [37]

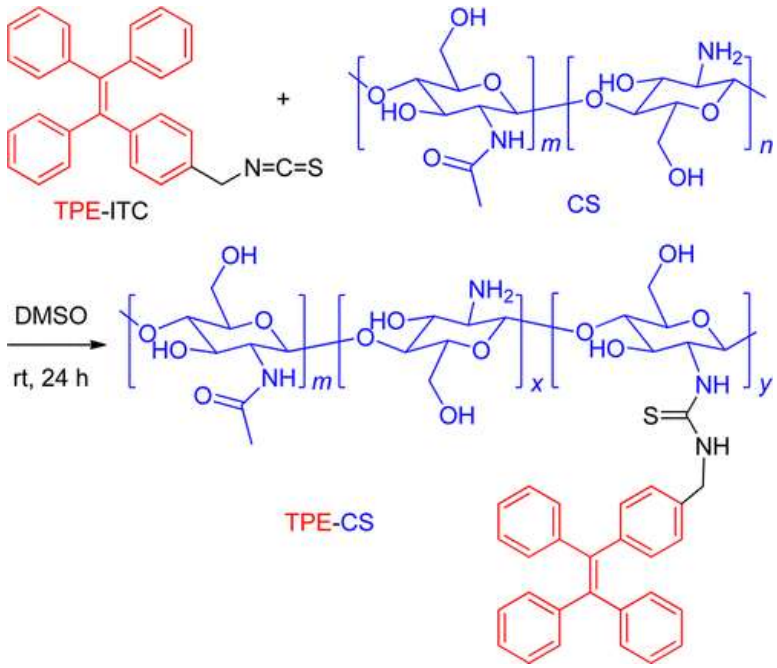

Figure 18. Synthetic route for the formation of TPE-grafted chitosan conjugates based on an isothiocyanate-amino reaction. A methylene spacer is added to the ITC-TPE molecule to avoid unwanted interactions with chitosan's backbone. **[37]**

More advanced alternatives of the previous protocol have been developed by inserting TPE between chitosan's chains by disulfide crosslinking. The procedure yielded particulate systems with redox-responsiveness, due to the disulfide bond's presence, and with aggregation-induced emission properties, stemming from TPE in the micellar structure (Figure 19). The nanomicelles were further functionalized with biotin (EDC/NHS condensation) to ensure high uptake via endocytosis by human breast cancer cells (MCF-7). [38]

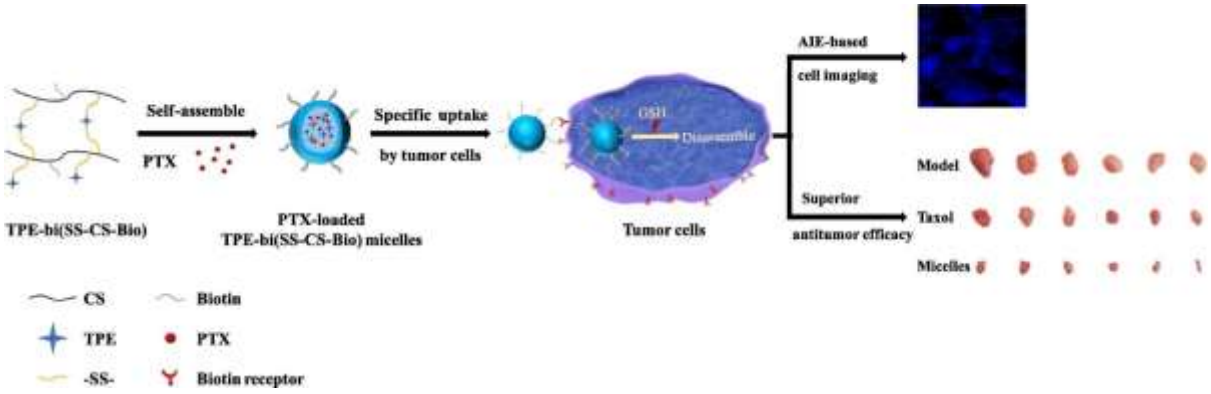

Figure 19. TPE-bi(SS-CS-Bio) nanomicelles with aggregation-induced emission and redox-responsiveness in MCF-7 cancer cells. **[38]**

Another endogenous stimulus of solid tumours that can be exploited for a responsive release strategy, is elevated levels of certain enzymes inside the TME. The hydrophilic copolymer CH_3O-PEG_{43}-b-PAA_{55} has been modified with TPE in the side chain to afford amphiphilic structures that form micelles via self-assembly in aqueous media (Figure 20). Due to the aggregation of TPE, strong fluorescence in the blue area with UV excitation was presented, along with responsiveness to esterase levels *in vitro*. Higher concentrations of esterase resulted in the dissociation of the micelles and as a result the quenching of the AIEgen's fluorescence. The chemotherapeutic drug doxorubicin was also loaded into the micelles and was successfully delivered inside the cancer cells due to the system's triggered release. TPE was accumulated near the nucleus of the cancer cells, as shown by confocal microscopy. The quenched fluorescence of TPE was observed, confirming the successful micelle dissociation inside the cancer cells and the delivery of doxorubicin. [39]

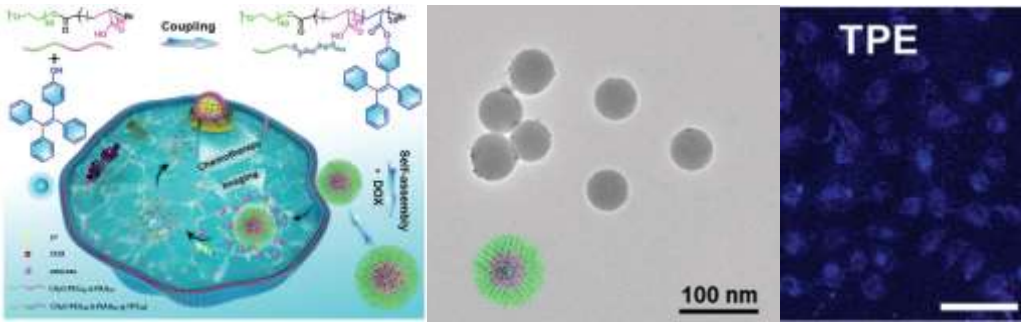

Figure 20. a) Schematic illustration of CH_3O-PEG_{43}-b-P(AA_{20}-g-TPE_{35}) micelles for cancer chemotherapy and aggregation-induced emission imaging. b) The produced nanomicelles with a mean diameter of 60 nm, as observed by Transmission Electron Microscopy c) TPE accumulates inside the cancer cells and its fluorescence is quenched as observed by confocal microscopy. **[39]**

Instead of the polymer's side chain, AIEgens can be directly incorporated into the copolymer's backbone. Two exemplary cases are the triblock polymers TPE-(PCL-*b*-$PEO)_2$ and TPE-(PEO-*b*-$PCL)_2$, which can be easily synthesized via a ring opening

polymerization reaction in only one step (Figure 21). The micelles are formed by dissolving each copolymer in DMSO and then dialyzing against water. This process yields TPE-containing micelles with an average size of 43.6 nm and 82.6 nm for TPE-(PCL-*b*-PEO)$_2$ and TPE-(PEO-*b*-PCL)$_2$, respectively. The difference in nanoparticle size is attributed to the different polymer arrangement in the amphiphilic structure, where in the latter case the hydrophilic PEG segment has acquired a loop-like configuration to be exposed to the aqueous media. Thus, it leads to larger cavities in the micelle structure, as shown in Figure 22. [40]

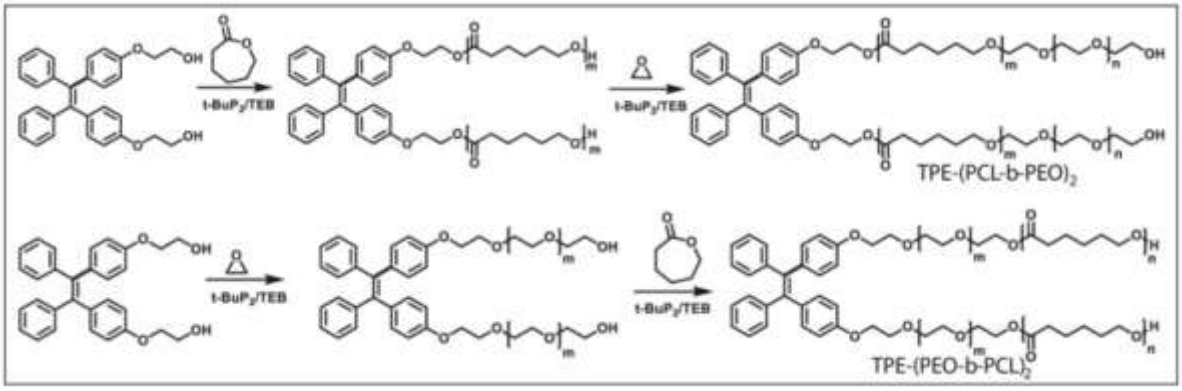

Figure 21. Ring opening polymerization for synthesizing the triblock copolymers TPE-(PCL-*b*-PEO)$_2$ and TPE-(PEO-*b*-PCL)$_2$ by using TPE-2OH as the initiator. **[40]**

The role of the chemical sequence in the triblock polymers, is also reflected in their behaviour as AIEgens. Due to the denser aggregation of the TPE moieties inside the micelle core, TPE-(PCL-*b*-PEO)$_2$ presented higher quantum yield than TPE-(PEO-*b*-PCL)$_2$. In addition, both polymeric micelles presented pH-responsive behaviour, since lower pH (5.5) accelerated significantly the release of the encapsulated chemotherapeutic drug (doxorubicin). This is explained by the protonation of the polymer in lower pH, and as a result the increased swelling of the micelles. Empty micelles showed high biocompatibility in normal healthy cells, as well as in HeLa and MCF-7 cancer cells. After loading doxorubicin in the micelles, cytotoxicity to cancer cells increased significantly due to the intracellular delivery of the drug. The position of the micelles in the cancer cells was visualized with confocal microscopy, where intense blue emission was observed near the nucleus. [40]

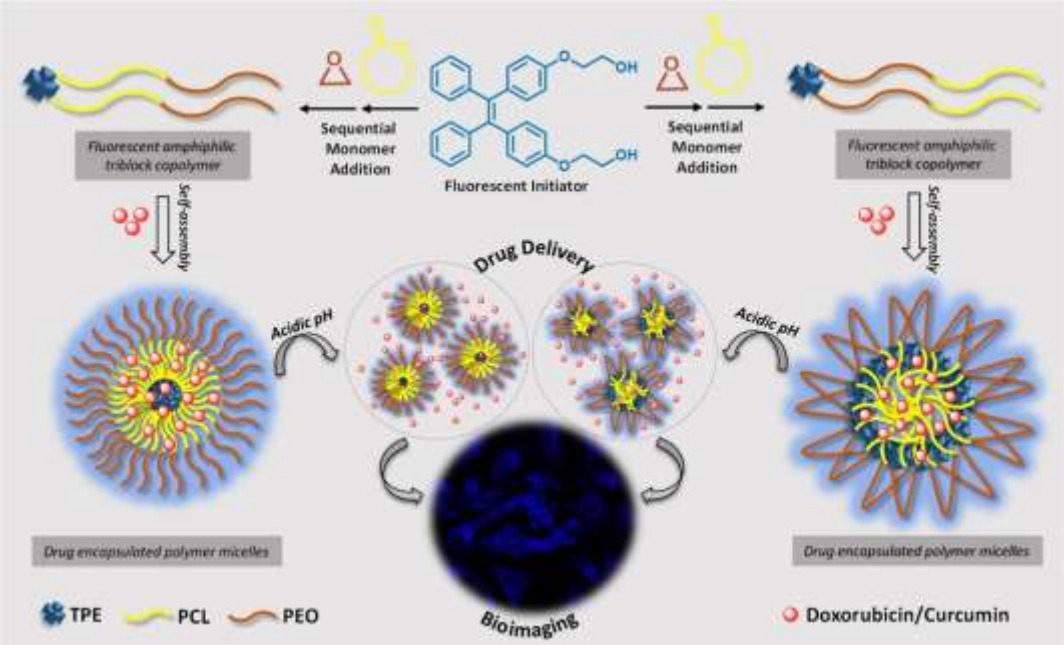

Figure 22. Illustration of the two different micellar structures of the triblock copolymers TPE-(PCL-*b*-PEO)$_2$ and TPE-(PEO-*b*-PCL)$_2$, and their aggregation-induced emission in cancer cells for bioimaging. **[40]**

3.1.3 Polymeric Micelles & Quantum Dots

Quantum Dots (QDs) are an alternative fluorescent probe for medical imaging that has been introduced the recent years. QDs are defined as semiconducting nanocrystals (2-20 nm) with intense photoluminescence and outstanding quantum yields. However, their administration *in vivo* faces difficulties due to their hydrophobic nature. To facilitate the dispersion of QDs in aqueous media and enhance their colloidal stability, amphiphilic copolymers can be used as a coating material. [41], [42]

To start with a simple example, the amphiphilic copolymer poly(ethylene glycol)-poly(D,L-lactide) (PEG-PLA) has been studied for the encapsulation of trioctylphosphine-coated CdSe/ZnS QDs. The copolymer and the QDs have been prepared by dispersing them in chloroform and mixing the two solutions. Upon evaporation of the organic solvent, water must be added to hydrate the film and yield the QD-loaded polymeric micelles (Figure 23). The obtained product presented outstanding colloidal stability in physiological media over the period of 24h, while the intense fluorescence of the QDs was maintained after their cellular uptake by cancer cells. [41]

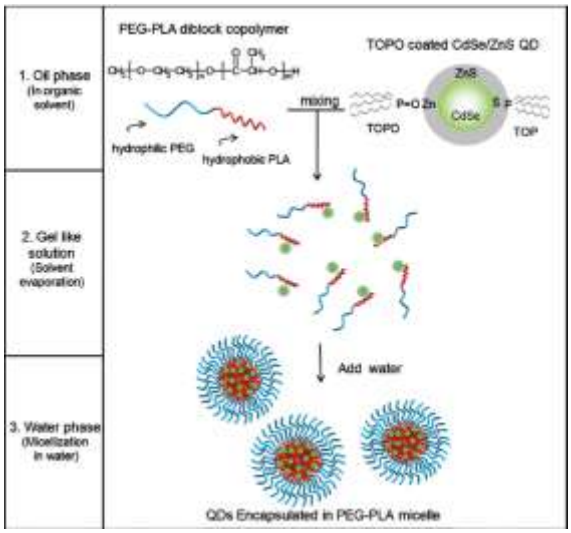

Figure 23. Preparation protocol for QD-loaded PEG-PLA BCP micelles. [41]

A more advanced version of the previous nanosystem has been developed, by using a pH-responsive multiblock copolymer to increase the selectivity of the contrast agent. The pH-responsive amidoamine-based polymer methoxy poly(ethylene glycol)-poly(β-amino ester/amidoamine)-dodecylamine (mPEG-PAEA-DDA) has been used for the formation of micelles and the encapsulation of core/multishell CdSe@ZnS/ZnS QDs, by a similar protocol as described above. The polymeric coating offers enhanced colloidal stability at physiological pH and prevents the leakage of toxic cadmium ions, rendering the product more biocompatible. The formulation was applied for the detection of cerebral ischemia by left middle cerebral artery occlusion in mice. Strong green fluorescence was observed in the ischemic section of the brain due to the accumulation of the nanosystem after 0.5 h post the injection. This is explained by the destruction of the blood-brain barrier due to the ischemic damage, that allows the intrusion of the nanoparticles inside the brain and thus the pH-triggered release of the encapsulated QDs (Figure 24). [42]

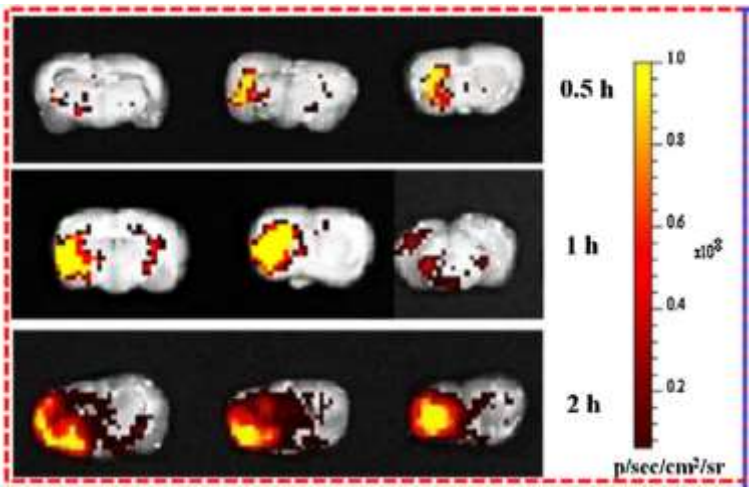

Figure 24. Cross-section fluorescence imaging of mice with cerebral ischemia after the administration of the pH-responsive system QDs@mPEG-PAEA-DDA. [42]

Table 2. Applications of block copolymer micelles in optical bioimaging.

Block copolymer	Probe	Responsiveness	Modality	Bioimaging	Ref.
PEG-PCL	Indocyanine green incorporated in micelle's core	-	NIR Fluorescence	NIR fluorescence imaging in cancer cells MCF-7 and mice.	[36]
PMPC-b-P (DEMA-*co*-SS-GEM-*co*-TPMA)	TPMA grafted on polymer backbone	Endosomal pH, Redox environment	Aggregation-induced Emission Fluorescence	Two-photon CLSM in 4T1 tumour cells.	[43]
TPE-Chitosan	TPE grafted on polymer via ITC-amino reaction.	Aggregation at higher pH (6.2)	Aggregation-induced Emission Fluorescence	Fluorescence microscopy in HeLa cancer cells.	[37]
TPE-bi(SS-CS-Bio)	TPE conjugated with chitosan vis disulfide crosslinking	Redox environment (GSH)	Aggregation-induced Emission Fluorescence	Confocal fluorescence microscopy in MCF-7 human breast cancer cells & 4T1 mice breast cancer cells	[38]
CH_3O-PEG_{43}-b-P(AA_{20}-g-TPE_{35})	TPE conjugated with copolymer in the side chain	Esterase	Aggregation-induced Emission Fluorescence	Confocal fluorescence microscopy in MCF-7 cancer cells	[39]
TPE-(PCL-b-PEO)$_2$ and TPE-(PEO-b-PCL)$_2$	TPE conjugates inside the triblock polymer	pH	Aggregation-induced Emission Fluorescence	Confocal fluorescence microscopy in HeLa cancer cells	[40]
Linear Dendritic PCL-PAMAM	Indolizine Cyanine Dye	-	NIR Fluorescence	Cell imaging in HEK cytoplasmic bodies	[44]
QDs@PEG-PLA	QDs encapsulated into micelle core	-	Fluorescence	Confocal fluorescence microscopy in HeLa cancer cells	[41]
QDs@mPEG-PAEA-DDA	QDs encapsulated into micelle core	pH-triggered (<6.8) targeting	Fluorescence	Fluorescence imaging in mice with cerebral ischemia	[42]

3.2 BCP Micelles in Magnetic Resonance Imaging

3.2.1 BCPs as platforms for the encapsulation of CAs

Polymer micelles are excellent candidates for the encapsulation of paramagnetic chelates inside their structure. The confinement of the chelate inside the micelle, leads to reduced rotation mobility, and by extension increased relaxivity of the paramagnetic element. [45] In combination with the pH-responsiveness of certain BCP micelles (e.g. polymers containing blocks of PAA), novel MRI probes can be developed with high selectivity to the biological site. In such cases, the acidic pH of the tumour microenvironment induces the collapse of the micelle structure, leading to significant enhancement of the MRI contrast when the nanoparticles enter the site of interest. [45]

The encapsulation of the MRI probe into the BCP micelle nanoparticles, can be achieved through the self-assembly between the paramagnetic ions and the polymer in solution or by covalently attaching the paramagnetic chelate to the polymer. Regarding the first case, common chelate groups, such as DOTA (1,4,7,10-tetraazacyclododecane-1,4,7,10-tetraacetic acid), can be attached to polymers containing primary amino groups (e.g., PEG-PLys). [46] Then, the paramagnetic element (e.g., Gd^{3+}) is dissolved in the solution and interacts spontaneously with chelator-modified polymer. Alternatively, the entire chelator complex containing the paramagnetic moiety, can be covalently grafted on the polymer block, usually via NHS/EDC coupling. [45]

Regarding superparamagnetic agents, such as SPIONs, their encapsulation in the hydrophobic core of BCP micelles, leads to an increased ratio of tranverse versus longitudinal relaxivity ($^{r_2}/_{r_1}$). This way, the efficacy of SPIONs as T2 CAs in MRI is significantly enhanced offering images with high contrast (negative contrast in this case). [47]

The contrast enhancement offered to the micellar carrier by the CA is highly related to the overall configuration of the nanosystem. If a paramagnetic CA, such as Gd, is entrapped into the hydrophobic core of the micellar structure, then the offered T1-shortening effect will be quenched. However, when the micellar vehicles start dissociating in the TME, the CA is going to be freed and enabled to interact with the surrounding water molecules, offering a strong MRI signal. This requires that the dissociation procedure happens inside the tumour tissue and not in the bloodstream, where the individual polymeric chains are going to be rapidly excreted resulting to very low signal. The Enhanced Permeability and Retention effect (EPR), that is a characteristic of the faulty lymphatic drainage system of solid tumours, allows the accumulation of BCP nanoparticles inside the TME resulting in very high imaging signals (passive targeting as shown in Figure 25). This way, a lower dosage of the nano-sized CA can be used to achieve very high contrast in the area of interest. [48]

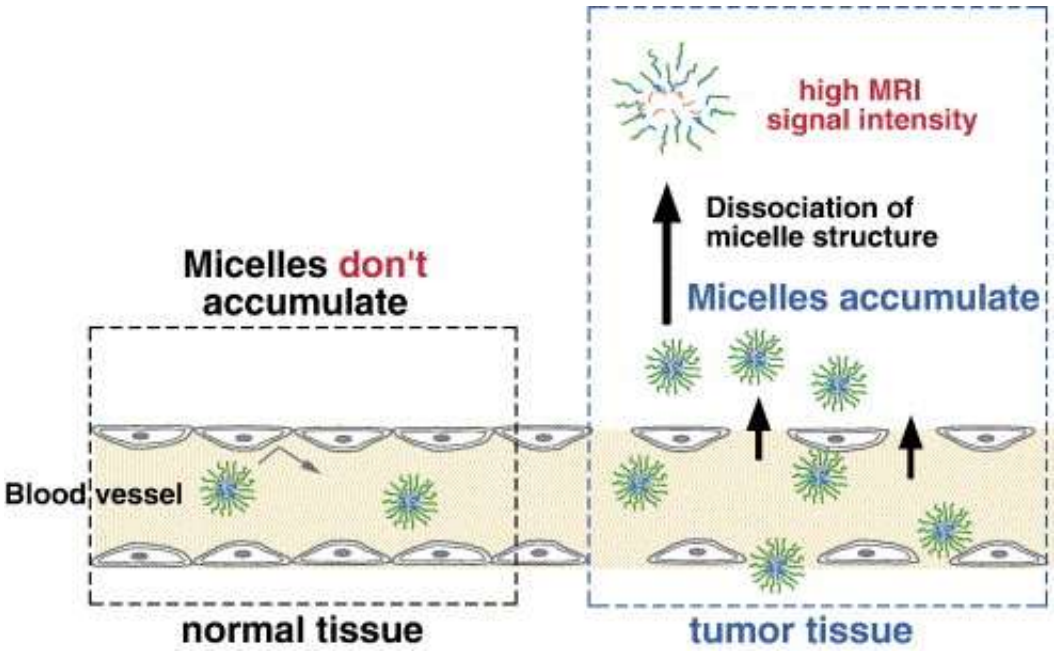

Figure 25. BCP micelles as CAs in tumour MRI with passive targeting. **[48]**

On the other hand, if the paramagnetic CA is conjugated on the hydrophilic blocks of the micelles' surface instead of the hydrophobic core, then the relaxivity of the CA is maintained since it is still exposed to the surrounding water molecules (Figure 26B). [49]

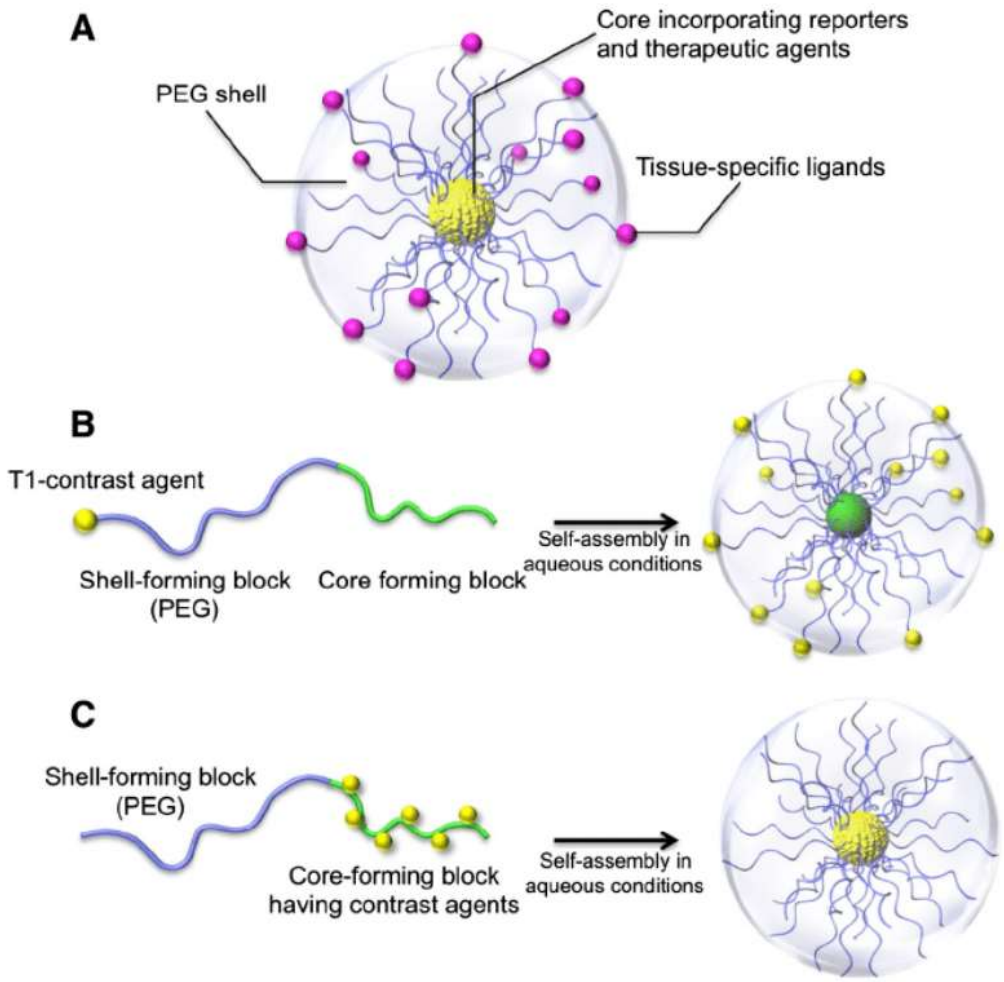

Figure 26. A) General scheme of amphiphilic BCP micelles bearing targeting ligands on their hydrophilic outer surface for site-specific medical imaging. B) Conjugation of the T1-shortening MRI CA on the hydrophilic block, leaving the CA exposed to the surrounded water molecules. C) Conjugation of the T1-shortening MRI CA on the hydrophobic block and entrapment inside the micelle's core. **[49]**

Regardless the CA position, a different approach for achieving high accumulation of the micelles in the biological site, is functionalizing the hydrophilic surface with biological recognition moieties (active targeting). For instance, folic acid is a very common surface modification ligand for nanoparticles, since it presents high affinity to the folate receptors in tumour cells. Figure 27 depicts a characteristic example of folate functionalized PEG-PCL micelles for the encapsulation of hydrophobic modified SPIONs. The presence of the targeting ligand folate on the micelles' surface enhanced significantly their *in vivo* performance as CAs for tumour cells. This proved the superiority of active targeting in comparison to the passive accumulation of the nanoparticles through the EPR effect. [47]

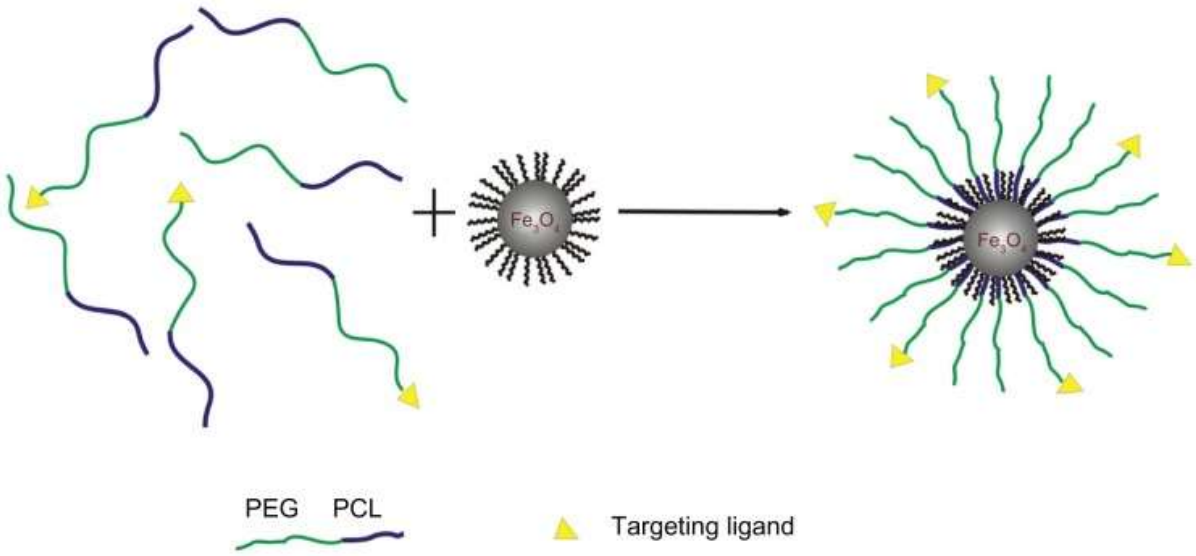

Figure 27. Folate-functionalized PEG-PCL BCP micelles for the encapsulation of hydrophobic SPIONs. **[47]**

To avoid long-term toxicity (nephrogenic system fibrosis) due to the accumulation of the Gd-loaded micelles in the liver and the spleen, other paramagnetic metals should be considered for the development of nano-sized MRI CAs. Manganese (II) is a biogenic paramagnetic metal that has been proposed by the scientific community for substituting gadolinium in MRI clinical practice. An azide-functionalized lauric acid-dextran nanomicelle system has been used for the covalent conjugation of a manganese complex via click chemistry. The rigid structure of the complex (triazole ring) and its immobilization onto the dextran's surface prolonged the rotational correlation time of manganese (τ_R), leading to enhanced T1 relaxivity. [50]

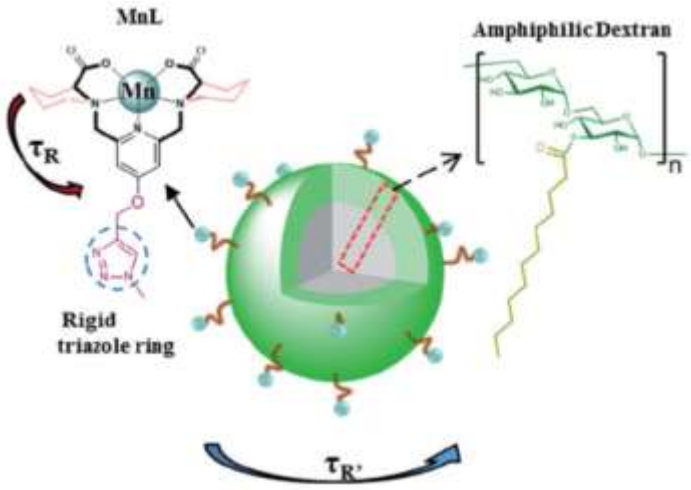

Figure 28. Conjugation of a manganese complex onto the surface of lauric acid-dextran BCP micelles via click-chemistry. **[50]**

The nanomicelles exhibited enhanced MRI contrast *in vivo* in Sprague-Dawley rats compared to the free manganese complex (Figure 29). By conjugating the complex on the nanomicelles' surface, the T1 relaxivity of magnanese increased from 4.8 to 13.3 $\mathrm{mmol}^{-1}\mathrm{s}^{-1}$. [50]

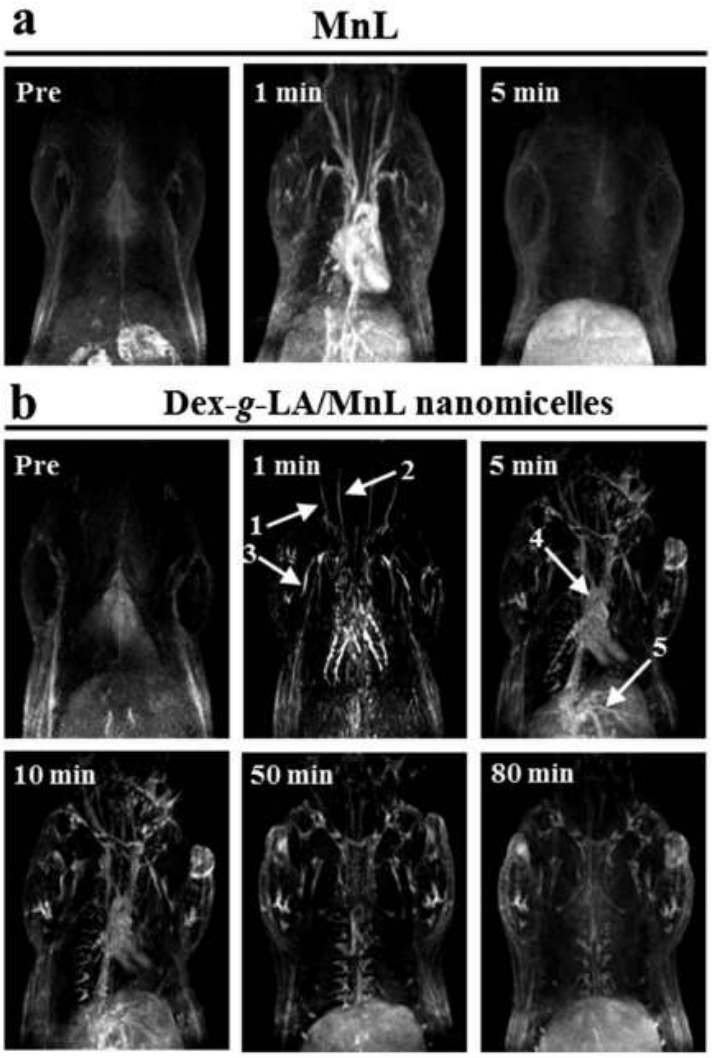

Figure 29. T1-weight MR images of Sprague-Dawley rats after the administration of the A) free magnanese complex, and B) the paramagnetic nanomicelles bearing the complex on their surface. **[50]**

3.2.2. BCPs in heteronuclear MRI (^{19}F,^{31}P)

To obtain images with ultra-high resolution and minimized background noise, different NMR-active nuclei such as ^{19}F or ^{31}P, have been investigated recently. To start with, ^{19}F is one of the most promising heteronuclear atoms with MRI-responsiveness, since it holds the 83% of the sensitivity of ^{1}H. Fluorine atoms in the human body are scarce, and those existing in tissues are immobilized with very short relaxation times. Thus, the background contrast is minimized in ^{19}F-MRI, generating images with high signal-to-noise ratios and quantifiable uptake. ^{19}F can be delivered to cells by its incorporation

in appropriate delivery systems, such as nanomicelles. ^{19}F- and ^{1}H-MRI can be combined to visualize the biological target with the accumulation of the fluorinated probe, while the anatomical details of the region can be obtained at the same time through the protons' relaxation. [51]

An example of BCP micelles developed for ^{19}F-MRI is the case of the hyperbranched amphiphilic fluorinated polymer presented in Figure 30, which is the product of co-polymerization of 4-chloromethyl styrene, lauryl acrylate (LA), and 1,1,1-tris(4′-(2″-bromoisobutyryloxy)phenyl)ethane. By transferring the synthesized polymer in the aqueous phase BCP micelles were formed, with diameters in the range from 3 to 8 nm as obtained by Transmission Electron Microscopy. As determined by phantom MRI *in vitro*, the relaxation times of the micelles were significantly shorter in comparison to conventional ^{19}F-MRI CAs, such as perfluorocarbons ($T_1 = 500$ ms and $T_2 = 65$ ms). The fluorinated probe generated images with very high signal-to-noise ratios. [52]

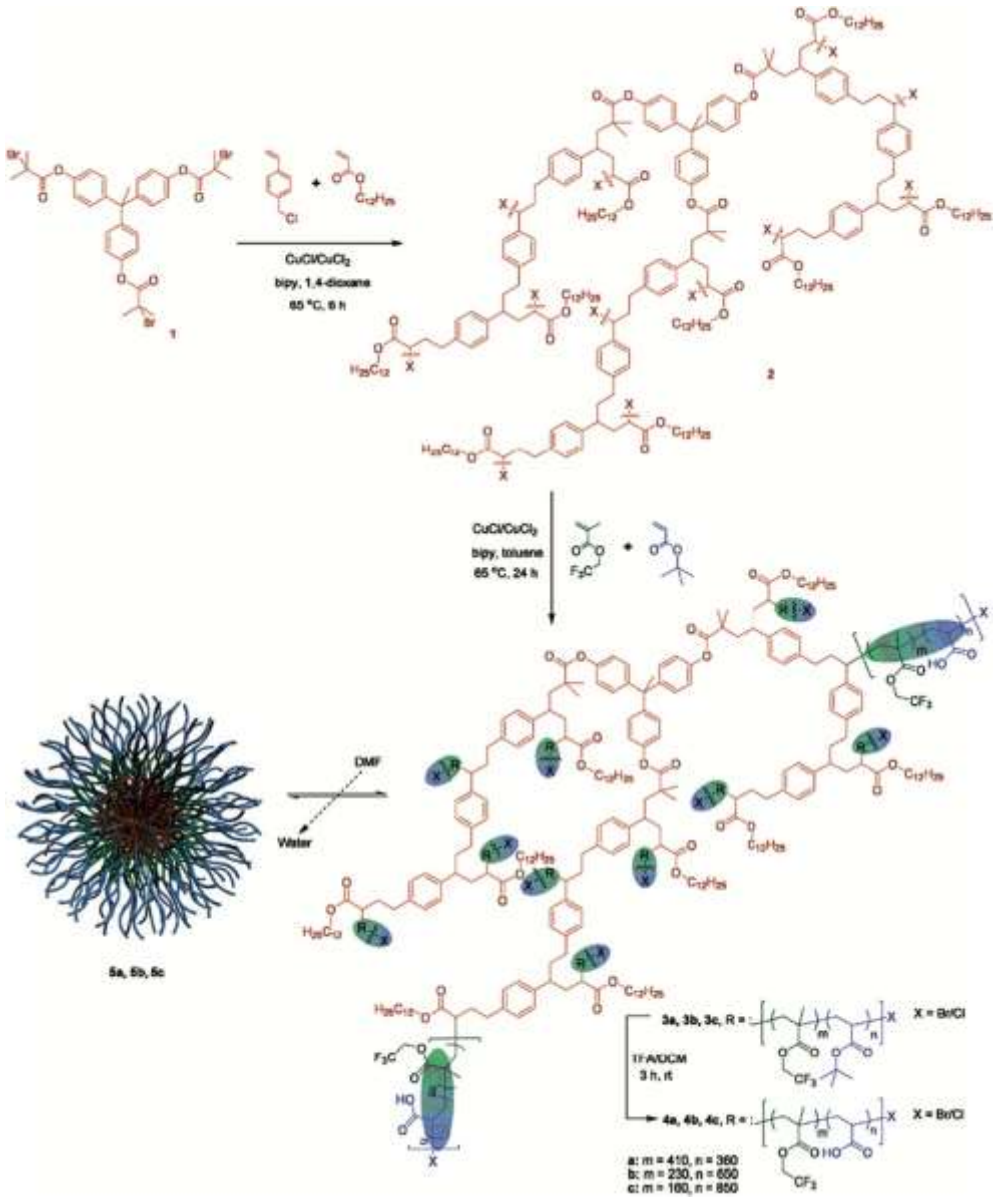

Figure 30. Synthesis of a hyperbranched fluorinated copolymer and the formation of BCP micelles in the aqueous phase. **[52]**

Fluorinated nanomaterials consist excellent candidates for developing novel MRI CAs, but their biodegradability is limiting their application *in vivo*. Due to the stable nature of the fluorinated bonds, these polymers are not easily decomposed by the human body, and they have presented unwanted organ deposition after their administration. On the other hand, ^{31}P is a naturally occurring element in the human body and the class of polyphosphoesters is emerging in the field of ^{31}P-MRI. However, the sensitivity of ^{31}P is relatively low compared to ^{19}F (only 7% of the ^{1}H sensitivity), and the background of the biological tissues presents intrinsic interference due the presence of natural phosphates. [53]

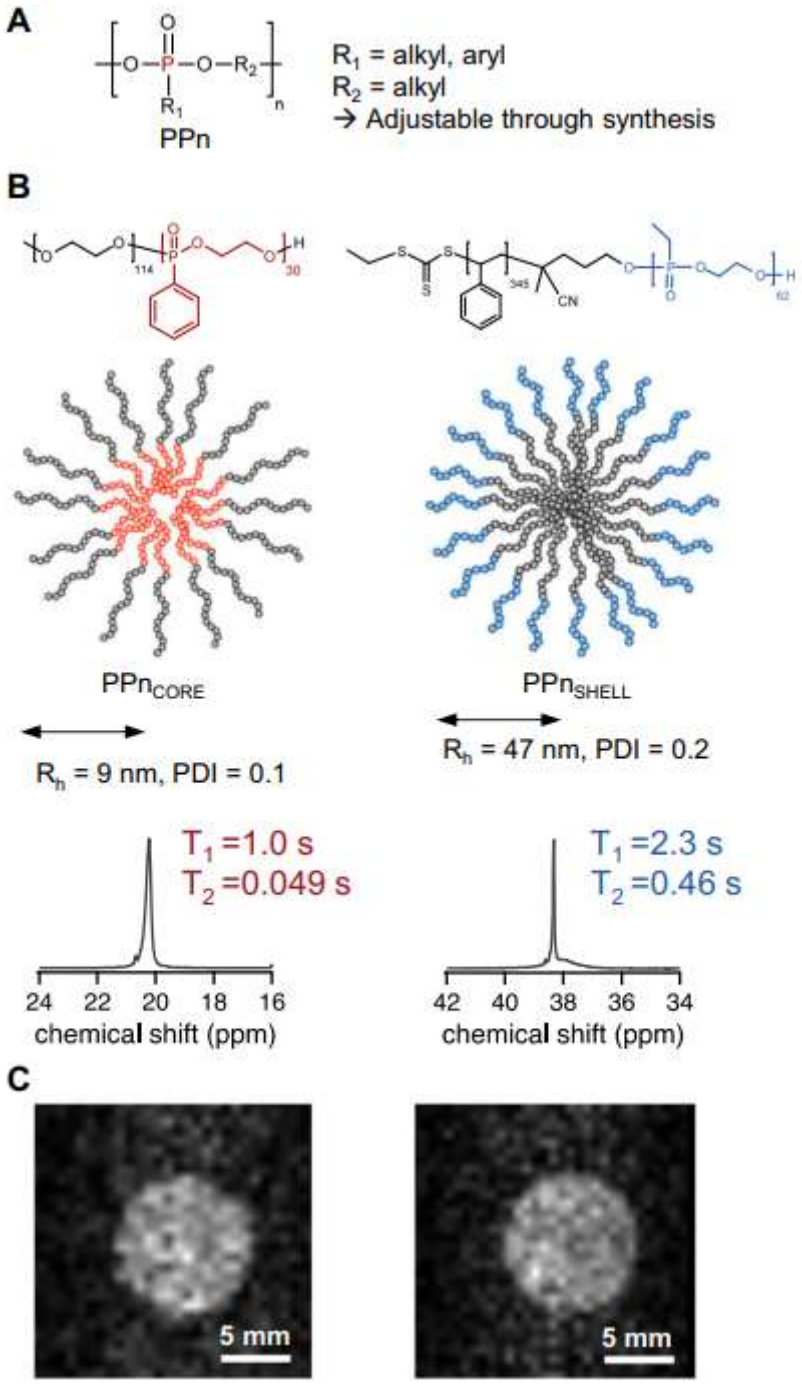

Figure 31. A) General chemical structure of polyphosphonates, B) Chemical structures of the two BCP polymers and the two corresponding micelles with ^{31}P located in the core and the shell of the nanoparticles. C) ^{31}P-MRI phantom images of aqueous suspensions of the two micellar systems. **[53]**

Polyphosphonates can be designed to accommodate ^{31}P atoms in the core or the shell of their corresponding micelles in aqueous solution (Figure 31). In both cases adequate CAs can be synthesized for ^{31}P-MRI, with a slightly higher relaxivity in the case of ^{31}P being in the hydrophilic shell of the micelles where higher mobility is achieved. To further increase the relaxivity, both the hydrophobic and the hydrophilic segments can be designed to host phosphonate groups and finally yield gradient

copolymer micelles. The gradient micelles were successfully used in vivo for ^{31}P-MRI in *Manduca sexta* caterpillars (Figure 32). By overlaying the obtained ^{1}H- and ^{31}P-MR images, it is apparent that polyphosphonate micelles can be used as an MRI CA with high biocompatibility and adequate contrast. [53]

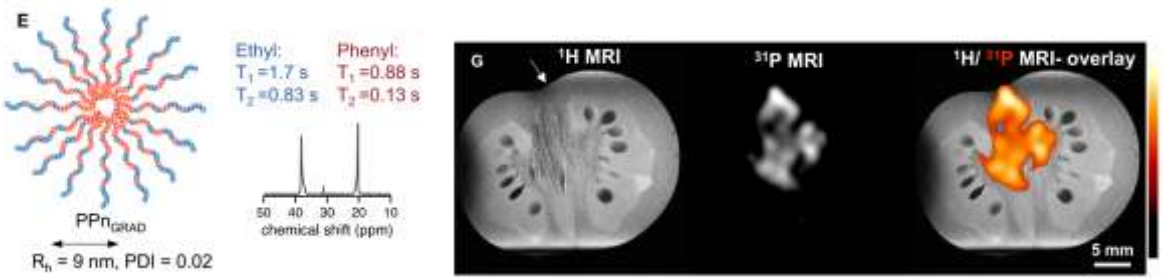

Figure 32. The structure of the gradient BCP micelles with phosphonated moieties in the core and the shell of the nanoparticles (left), and the in vivo ^{1}H- and ^{3}1P-MR images in *Manduca sexta* caterpillars, where the area of injection can be visualized by the accumulation of the nanomicelles (right). [53]

3.2.3. BCPs in CEST MRI

Interestingly, BCP micelles have been also applied in CEST MRI. Specifically, poly(ethylene glycol)-b-poly[2-(diisopropylamino)ethyl methacrylate] (PEG-b-PDPA) micelles containing ionizable tertiary amine moieties, have been used in a pH-responsive approach for CEST imaging. The pH-responsive characteristic of the developed system stems from the protonation of the PDPA polymer blocks rending them hydrophilic in lower pH (<6.5). This way the assembly of the micelles is resolved, and the polymer chains are dissolved freely in the dispersion media. Thus, CEST signal can observed in biological sites with acidic pH, where the micelle dissolution is promoted thermodynamically. [54]

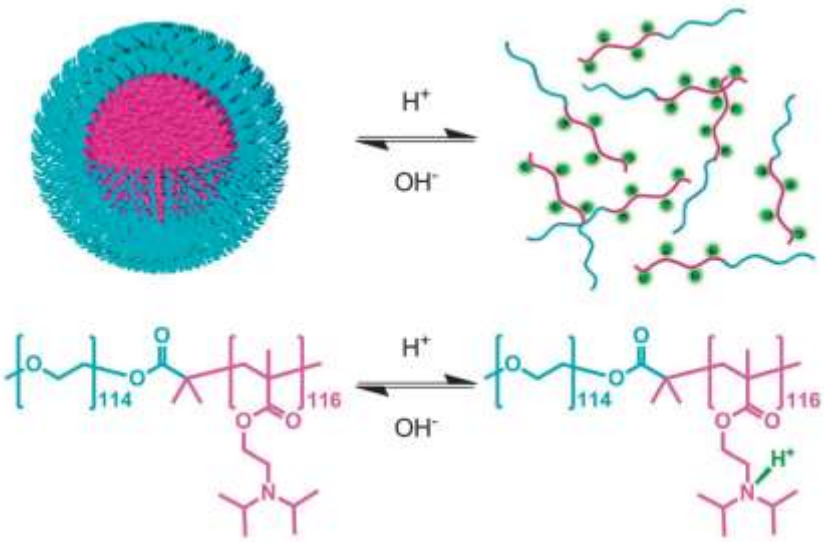

Figure 33. PEG_{114}-b-$PDPA_{116}$ micellar system for pH-responsive CEST MRI. **[54]**

Table 3. Applications of block copolymer micelles in ^{1}H-MRI.

Block copolymer	Probe	Incorporation	Responsiveness	Modality	Relaxivity ($mM^{-1}s^{-1}$)	Ref.
PS-b-PAA	Gd-DO3A	NHS/EDC Coupling	pH	T1	30.49 at pH=4.0	[45]
PEG-P(Lys-DOTA-Gd)-PAA PICs	PEG-P(Lys-DOTA-Gd)	Coordination with DOTA-modified polymer	pH	T1	5.6–7.3 at 9.4 T	[46]
SPIONs@mPEG-PLA/CS	SPIONs	Self-assembly of SPIONs inside micelle's core	-	T2	111.7	[55]
SPIONs@PEG-PCL-folate	SPIONs	Self-assembly of SPIONs inside micelle's core	-	T2 (r_2/r_1=78)	110	[47]
Multi-arm star H40-PCL-b-P(OEGMA-Gd-FA)	Gd-DOTA	Click chemistry	-	T1	18.14	[56]
PEG-P(Asp(DTPA-Gd)	Gd-DTPA	Coordination with DTPA-modified polymer	-	T1	2.1-3.6	[48]
h-P(CPTM-*co*-DOTA(Gd))-*b*-P(OEGMA-*co*-GPMA)	Alkynyl-Gd-DOTA	Click reaction with hyperbranched polyprodug core	GSH	T1	35.97 at 20 mM DTT	[57]
Azide-functionalized Lauric acid-dextran	Mn (II) Complex	Click chemistry	-	T1	13.3	[50]

3.3 BCP Micelles in PET Imaging

Polymer micelles have been used in radiolabelling for PET imaging. A representative example is the application of the triblock copolymer CB-TE2A–conjugated poly(ethylene glycol)-b-poly(hydroxyethyl methacrylate)-b-poly(methacryloyloxyethoxy-4-methylcoumarin) (PEG-PHEMA-PCMA) in ^{64}Cu radiolabelling. The micelle core was consisted of 4-methylcoumarin and was used in cross-linking of the core via UV irradiation after the micelle formation in aqueous solution. Regardless the cross-linking procedure micelles exhibited similar biodistribution behaviour in both cases with long circulation times (with a circulation half-time around 20 hours in mice). PET/CT imaging was conducted in tumour-bearing mice. Radiolabelled micelles delivered ^{64}Cu with a slower and steadier state, compared to the administration of the free radioisotope. [58]

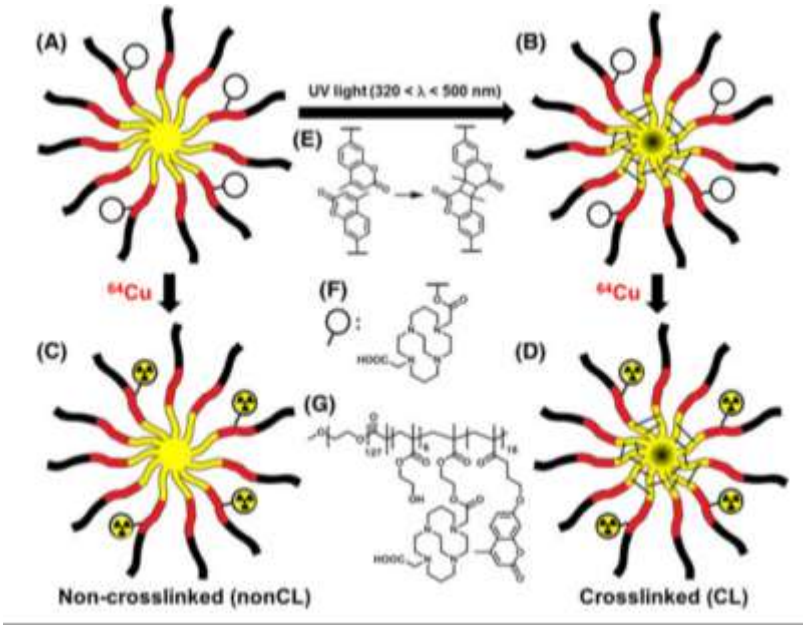

Figure 34. Radiolabelling of PEG-PHEMA-PCMA BCP micelles with ^{64}Cu. A) Non-cross-linked micelle without the radioisotope. B) Non-labelled micelle with cross-linked core via UV irradiation. C) ^{64}Cu-labelled non-cross-linked micelles. D) Cross-linker micelles labelled with ^{64}Cu. **[58]**

A more sophisticated approach has been proposed that involves the radiolabelling of unimolecular PAMAM-P(LA-Hyd-DOX)-b-PEG micelles. Doxorubicin was conjugated with the hydrophobic poly-L-aspartate segment via pH-labile hydrazone bond. The external surface of the micelles was functionalized with the F3 peptide for tumour targeting and with a chelating agent to host the radioisotope ^{64}Cu. The micelles exhibited enhanced radiochemical stability and facilitated the selective accumulation (active targeting and EPR effect) of the radioisotope inside the TME of breast tumour-bearing mice. The absorption of the nanomicelles was limited in healthy tissues (bones, muscles, brain), while some radioisotope quantity could be found in the liver, the spleen and the kidneys due the nanoparticle excretion process. [59]

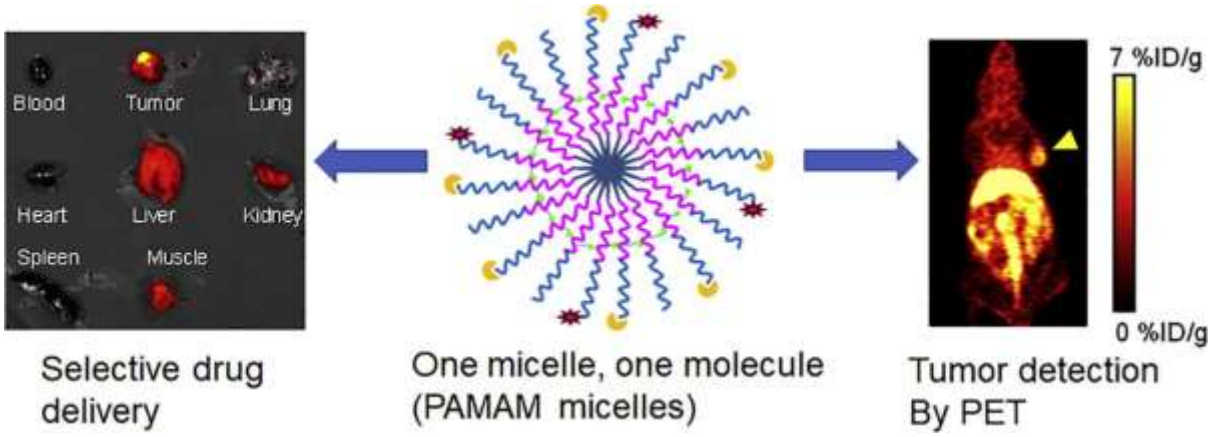

Figure 35. PAMAM-P(LA-Hyd-DOX)-b-PEG micelles radiolabelled with ^{64}Cu for targeted tumour PET imaging. **[59]**

3.4 BCP Micelles in CT Imaging

The hydrophobic segment of BCP micelles can be chemically modified with iodine-containing molecules for the fabrication of micellar CT contrast agents. The triblock copolymer mPEG-PA-PLL has been used in such a case, by conjugating 2,4,6-triiodobenzoic acid onto the amine groups of the polylysine block via a condensation reaction. The iodinated moieties were accumulated inside the micelle's core after the self-assembly process in water. This system was applied in blood pool CT imaging in rats with enhanced contrast (150 HU in the heart, 57 HU in the liver and 90 HU in the spleen, 120 minutes after the injection). [60]

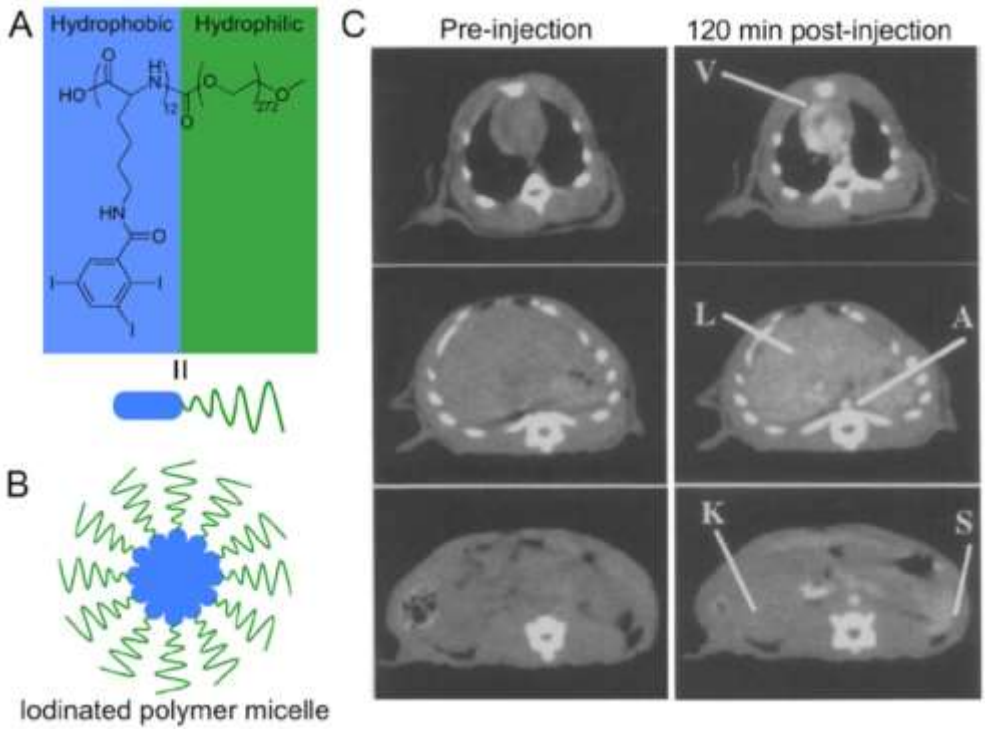

Figure 36. A) Chemical structure of mPEG-PA-PLL modified with 2,4,6-triiodobenzoic acid. B) Micellar structure of the amphiphilic polymer in water. C) Blood pool CT imaging in rats before and 120 minutes after the injection with the iodinated micelles. **[60]**

A different approach has been recently proposed that involves the synthesis of an iodinated polymer and then the co-assembly with an amphiphilic polymer to form the micelles. Figure 37 presents all the different synthetic pathways that have been used for obtaining iodinated BCP and surfactant micelles for CT imaging through the co-assembly process. [61] To start with, polyvinyl alcohol has been modified with 2,3,5-triiodobenzoyl chloride via an esterification reaction to afford the iodinated polymer (Figure 37A). The polymer along with PCL-b-PEG were dissolved in the organic solvent (THF) and the micelles were formed by dropping the mixture into the aqueous phase (nanoprecipitation). The dense brush-like configuration of PEG chains on the surface of the nanomicelles (with a diameter around 150 nm), afforded a blood contrast agent with enhanced circulation time and signal (over 200–250 HU in the abdominal aorta and the heart) for the visualization of the cardiovascular system of rats. [62] In a different study, polyvinyl phenol was iodinated via electrophilic substitution and co-assembled with the diblock copolymer PS-b-PEG (Figure 37B). The resulting micelles, with their size ranging from 35 nm to 130 nm, presented high iodine content and enhanced contrast for X-ray phantom imaging *in vitro*. [63]

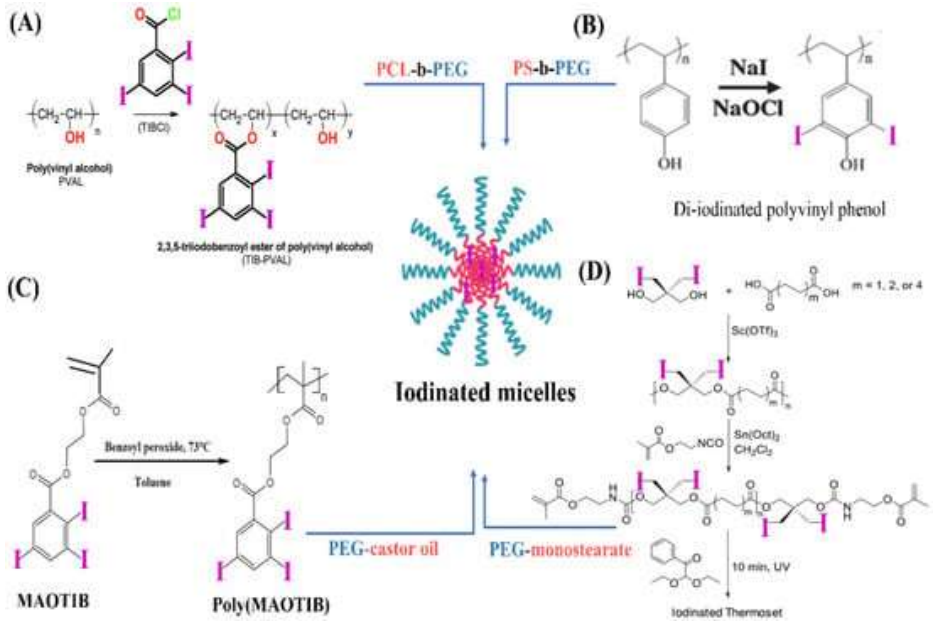

Figure 37. A) Iodinated polyvinyl alcohol co-assembled with PCL-b-PEG for cardiovascular blood pool CT imaging. B) Iodinated polyvinyl phenol co-assembled with PS-b-PEG for CT imaging. C) Iodinated polymer Poly(MAOTIB) co-assembled with the surfactant castor oil-PEG35 for blood pool imaging. D) Iodinated polyester co-assembled in micelles with surfactant lecithin and PEG-monostearate. **[61]**

3.5 BCP Micelles in Multimodal Imaging

Dual CT/Fluorescence Imaging

Synergistic imaging involves the combination of at least two different modalities, with aim to alleviate their intrinsic limitations and afford higher quality visualizations of medical interest. For example, CT imaging offers crucial anatomical details but presents low sensitivity. This can be resolved by combining CT imaging with another modality with higher sensitivity and quantitative character, such as fluorescence or PET imaging. Regarding fluorescence, conventional or novel fluorophores, such as AIEgens, can be incorporated into iodinated micelles to afford CAs with dual function. Another interesting approach involved the use of a semiconducting polymer as the NIR fluorescence probe, since they usually exhibit high quantum yields and be further used for photodynamic therapy in theranostic applications. The iodinated amphiphilic BCP PEG-PHEMA-I, along with the semiconducting polymer PCPDTBT have been used for the development of X-ray attenuating fluorescent micelles (Figure 38). The micelles were synthesized by dissolving the micelles in THF and then adding water to the mixture (co-precipitation). The developed system (with diameters around 20-30 nm) was used in image-guided photodynamic therapy, given that the semiconducting polymer generated singlet oxygen upon irradiation, which was enhanced by the heavy atom effect due to the presence of the iodinated block polymer in the micelles. [64]

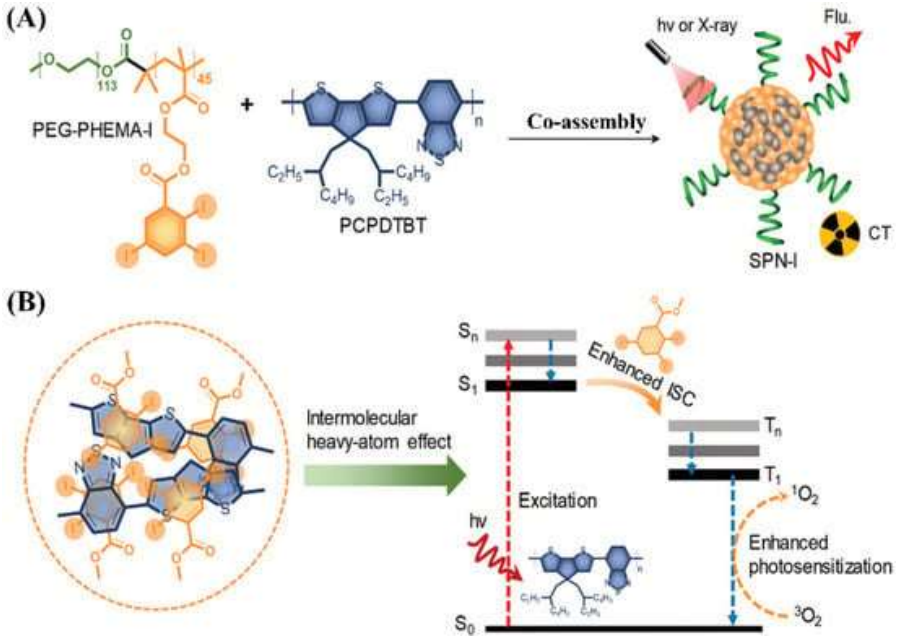

Figure 38. A) Co-assembly of the iodinated BCP PEG-PHEMA-I and the NIR-absorbing semiconducting polymer PCPDTBT into dual CT/fluorescent micelles. B) The presence of the iodinated polymer in the micelle's core enhanced the photodynamic efficacy of PCPDTBT due to the heavy atom effect. **[61]**, **[64]**

The performance of the fluorescent iodinated micelles was investigated in vivo with tumour bearing c57bl/6 male mice. According to the images obtained via NIR fluorescence imaging, the tumour site can be visualized in only 1 hour after the administration of the micelles, due to the nanoparticle accumulation through the EPR effect. Maximum accumulation in the tumour was observed after 48h (reaching 80 HU), which is explained from the long circulation time and stability of the particulate system. In the case of CT images only the bone structure can be observed up until the first 4h, when the tumour starts to be visualized due to the accumulation of the iodinated micelles. This result proves that the higher sensitivity of fluorescence imaging is acting complimentary with CT for the earlier detection of the tumour site. [64]

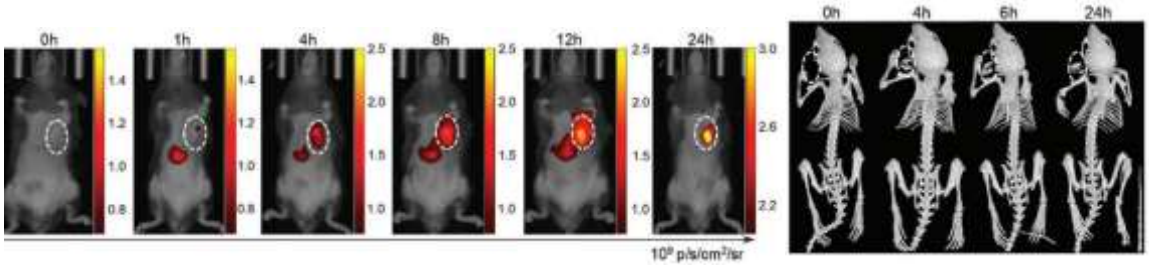

Figure 39. A) NIR fluorescence images of tumour-bearing mice after the administration of the BCP micelles. B) CT images of tumour-bearing mice in different time frames after the injection with the nanomicelles. **[64]**

Dual Fluorescence/MRI

The quantitative character of fluorescence imaging and the anatomical details provided by MRI, can be combined to provide outstanding results in visualizing biological tissues. Fluorescence imaging and MRI can be conducted at the same time by rationally designing a micellar system. For example, this can be achieved by incorporating hydrophobic SPIONs and a fluorophore inside the core of an amphiphilic BCP micelle system. The telodendrimer polymer mPEG-b-dendritic oligo-cholic acid (mPEG-Lys3-CA4) has been used for this purpose (Figure 40). The micelles were synthesized by dissolving the polymer, the fluorophore (Nile Red) and the SPIONs (<40 nm) in a mixture of solvents, and then slowly adding the organic phase to an aqueous solution. The solvent was evaporated, and the micelles were afforded in the aqueous dispersion. The encapsulation of SPIONs into the micelle's core increased their magnetic transverse relaxivity, and as a result their contrast in T2-weighted MRI as proven by phantom *in vitro* experiments. [65]

Figure 40. Illustration of the mPEG-Lys3-CA4 micelles for the encapsulation of ultra-small SPIONs and the fluorophore Nile Red. **[65]**

In addition, the nanomicelles presented increased uptake by Raw264.7 macrophage cells, as confirmed by confocal fluorescence microscopy with Nile red's strong emission (Figure 41). Given that the cancerous lymph nodes possess less macrophage cells, and as a result decreased ability for nanoparticle uptake, these results are very promising for the development of a macrophage-targeted imaging approach that will allow their visualization. Thus, the developed nanosystem possesses outstanding properties and performance to be further applied in the detection of metastatic malignant lymph nodes, given the high sensitivity offered with fluorescence/MRI. [65]

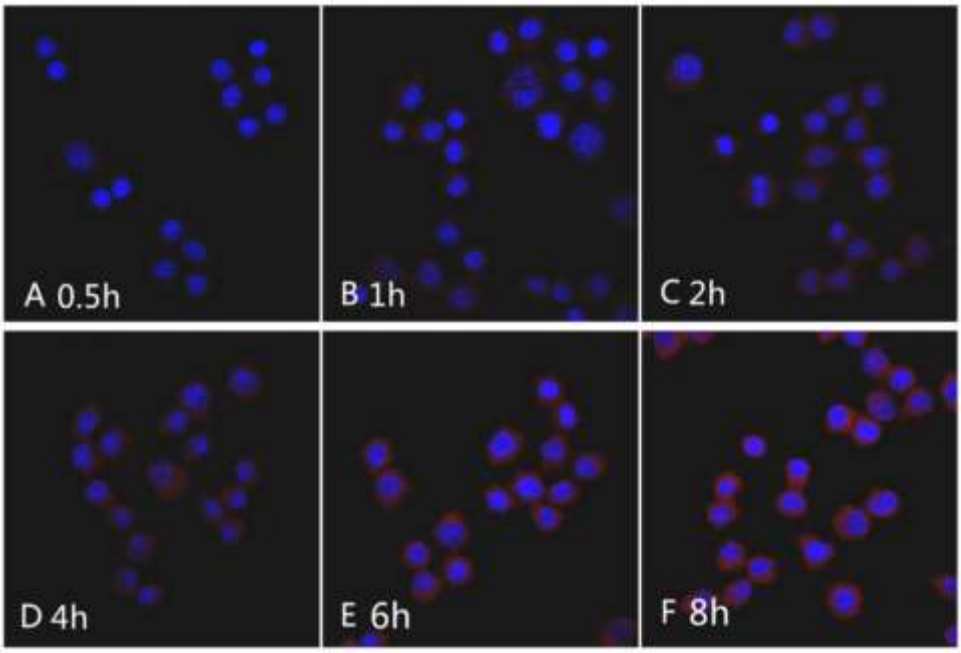

Figure 41. Cellular uptake of the NileRed/SPIONs@mPEG-Lys3-CA4 nanomicelles by Raw264.7 macrophage cells (the nucleus of the cells was stained blue with DAPI). **[65]**

Dual PET/MRI

By combining the outstanding anatomical resolution of MRI with the high sensitivity and quantifiable character of PET imaging, the intrinsic disadvantages of each modality are reduced. As discussed above, BCP micelles can be specifically designed as nanoplatforms for combined PET/MRI. The two block copolymers PBD-b-PEO and PBD-b-PAA have been used to synthesize amphiphilic micelles via their co-assembly in water. The carboxylic moieties of the polyacrylic acid segments were used to covalently conjugate a chelator named deferoxamine via a condensation reaction. Deferoxamine can efficiently coordinate with Fe^{3+} and Zr^{4+} ions. This way, the MRI-traceable Fe^{3+} ions and the PET radioisotope ^{89}Zr can be incorporated into the same micellar system (Figure 42). ^{89}Zr is known for its high specific activity (3 GBq/mg) and its applicability in prolonged circulation monitoring (3.3 d half-time). The paramagnetic Fe^{3+} ions are an ideal candidate for T1-weighted MRI, as it was determined by their transverse and longitudinal relaxivities measurement. [66]

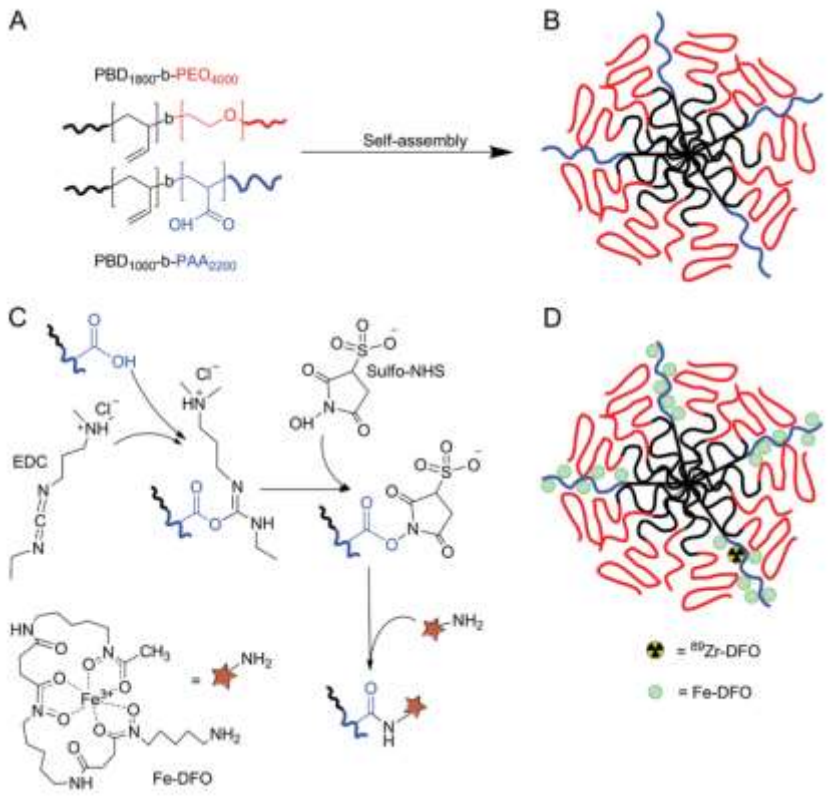

Figure 42. A) Chemical structure of the block polymers PBD-b-PEO and PBD-b-PAA. B) Co-assembly of the two polymers in micelles via thin film hydration. C) Conjugation of deferoxamine complexed onto the polyacrylic acid segments via a condensation reaction. D) Radiolabelled paramagnetic micelles for dual PET/MRI. **[66]**

The paramagnetic radiolabelled micelles (^{89}Zr/Fe-DFO-micelles) presented outstanding performance in tumour-bearing mice for dual PET/MRI. PET images revealed enhanced nanoparticle uptake by the tumours for the ^{89}Zr/Fe-DFO-micelles, as well as the control ^{89}Zr/Al-DFO-micelles (Figure 43: A,B,C). T1-weighted MRI (Figure 43: D,E,F) revealed an inhomogeneous accumulation of the nanomicelles in the tumour site, with an increased uptake near the tumour's periphery. This is attributed to the tumour's higher perfusion near its anatomical periphery in comparison to its necrotic core. After the procedure, the tumours were excised and analysed *ex vivo* via autoradiography. The results (Figure 43: G,H,I) confirmed the high intratumoural accumulation and inhomogeneous biodistribution profile that was concluded via the PET/MRI modalities. [66]

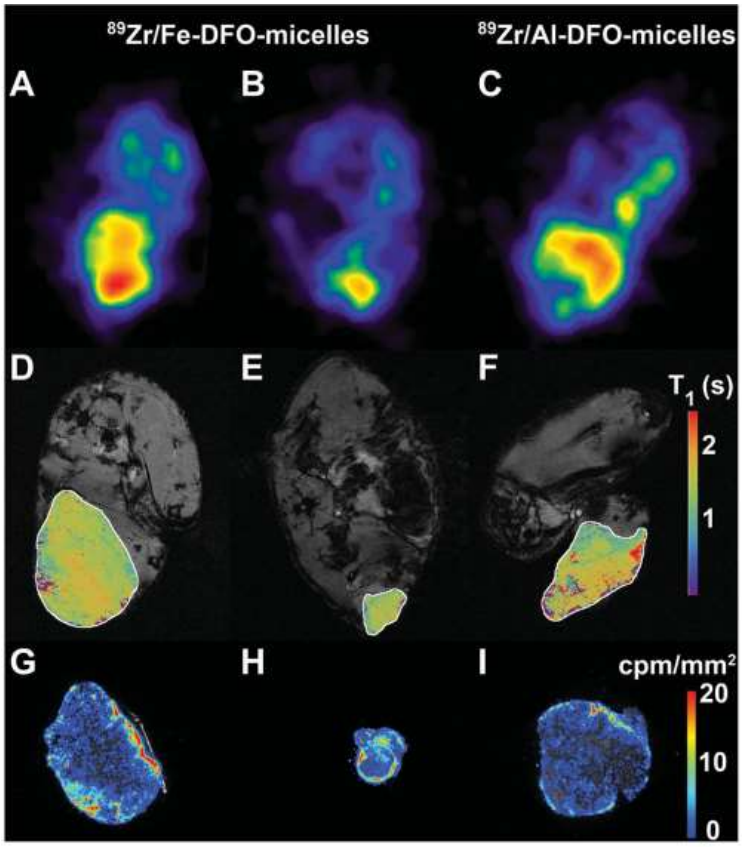

Figure 43. A,B) PET images of cross-sections throughout the limbs after the injection of the ^{89}Zr/Fe-DFO-micelles. C) PET images after the injection of the ^{89}Zr/Al-DFO-micelles. D,E,F) T1-weight MRI after the injection of the ^{89}Zr/Fe-DFO-micelles, G,H) Autoradiography images of the excided tumours after the injection with the ^{89}Zr/Fe-DFO-micelles, I) Autoradiography images of the tumour after the injection of ^{89}Zr/Al-DFO-micelles. **[66]**

Conclusions & Future Perspectives

BCP micelles are an extensively studied class of nanomaterials with outstanding properties, including enhanced colloidal stability, prolonged circulation times *in vivo*, chemical versatility, high loading capacity and responsiveness to external and/or endogenous stimuli. The above characteristics have brought BCP micelles in the forefront of nanomedicine, and specifically in nanoparticle-mediated bioimaging for the visualization of biological compartments, such as solid tumours. The imaging modalities include optical methods with non-ionizing radiation (fluorescence imaging), X-ray imaging and Computerized Tomography (CT), Positron Emission Tomography (PET) and Magnetic Resonance Imaging (MRI).

BCP micelles as colloidal structures with size under 200 nm accumulate inside the tumour microenvironment (TME) through the enhanced permeability and retention effect, that is attributed to the leaky vasculature of solid tumours. This way tumour imaging with enhanced contrast can be afforded, while minimizing the background noise. However, BCP micelles can be further modified to have cell-specific targeting to tumours. Firstly, by choosing the nature of the chemical reactions involved in synthesis, stimuli-responsive micellar nanoparticles can be developed for site-specific delivery of the loaded cargo that can be triggered by parameters, such as the acidic pH or the redox environment of the TME. Secondly, the surface of BCP micelles can be covalently modified with targeting ligands, such as folic acid, aptamers or antibodies to recognise the receptors of the cancer cells. In this case, the loaded cargo is delivered intracellularly affording enhanced contrast and sensitivity for imaging, especially when studied via microscopy.

Regarding optical bioimaging, the hydrophobic core of the BCP micelles can host a variety of organic probes used in fluorescence imaging, such as indocyanine green, achieving higher contrast and photostability. Especially, the case of NIR-excited fluorophores has presented the most interest by the scientific community, since NIR fluorescence exhibits deeper penetration in biological tissues. Recently, new generation probes have been studied in BCP micelles, such as aggregation-induced emission fluorogens (AIEgens) and conductive polymers. Most applications concern cancer cell imaging and drug release monitoring in cell lines via confocal microscopy. Less studies have been conducted about macroscopic imaging applications through fluorescence *in vivo*.

MRI is another imaging technique with interesting application of BCP micelles, since they can be used for the encapsulation of paramagnetic metals for T1-weighted imaging and superparamagnetic iron oxide nanoparticles (SPIONs) for T2-MRI. The most studied contrast agent is gadolinium (III), which is used in the clinical practice of MRI. Gadolinium can be incorporated into the core or the shell of the micelles and be delivered to the biological tissue of interest (usually cancer tumours) by passive or active targeting. Other paramagnetic metals, such as manganese (II) and iron (III) have been proposed as alternatives with higher biocompatibility to avoid the side effects presented by gadolinium. SPIONs can also be encapsulated inside the micelle's core due to their hydrophobic nature and afford T2-weighted images of

tumours or inflamed areas. The configuration of the polymer and the microenvironment around the contrast agent can be designed accordingly to enhance its relaxivity affording enhanced contrast images *in vivo*. Lastly novel MRI approaches, such as imaging via NMR-active heteronuclear atoms (e.g., ^{19}F, ^{31}P) and Chemical Exchange Saturation Transfer (CEST), have been examined with BCP micelles showing interesting preliminary results.

In addition, BCP micelles can be labelled with radioisotopes, such as ^{64}Cu and ^{89}Zr, and be used effectively in PET imaging *in vivo*. Their application mainly concerns the visualization of malignant tumours and the quantification of nanoparticle uptake. Lastly for CT imaging, BCP micelles can be synthesized by the co-assembly of iodinated polymers to afford X-ray attenuation contrast agents. Iodinated BCP micelles have mainly be used for blood pool imaging of the cardiovascular system and tumour imaging.

Due to the chemical versatility of BCP micelles, two or more contrast agents can be incorporated into the same nanoparticle system for enabling synergistic imaging. By combining two or more imaging modalities, their intrinsic limitations can be alleviated, and images of higher quality can be obtained. CT and MRI provide excellent information about the anatomical details of a biological region, but lack in sensitivity. On the other hand, PET and fluorescence imaging are known for their high sensitivity and quantitative character, but their spatial resolution is limited. So it is apparent that combining different modalities in the same nanosystem, such as MRI/PET, CT/fluorescence or MRI/fluorescence, more information can be obtained at the same time.

The future of BCP micelles in bioimaging concerns their ability to combine different modalities at once, which should be further investigated and expanded in a variety of biological targets, such as tumours, cardiovascular and pulmonary lesions, inflamed tissues, lymph nodes and others. However, their biodegradability and long-term accumulation in humans should be further studied to exclude the possibility of side effects and toxicity.

References

[1] G. Gaucher , M. H. Dufresne , V. P. Sant , N. Kang , D. Maysinger and J. C. Leroux , "Block copolymer micelles: preparation, characterization and application in drug delivery," *Journal of Controlled Release* , vol. 109, no. 1-2, pp. 169-188, 2005.

[2] G. Chen , Y. Wang , R. Xie and S. Gong , "A Review on Core–Shell Structured Unimolecular Nanoparticles for Biomedical Applications," *Adv Drug Deliv Rev,* vol. 130, pp. 58-72, 2018.

[3] S. M. N. Simoes, A. R. Figueiras, F. Veiga , A. Concheiro and C. Alvarez-Lorenzo, "Polymeric micelles for oral drug administration enabling locoregional and systemic treatments," *Expert Opin. Drug Deliv.*, vol. 12, no. 2, pp. 297-318, 2015.

[4] M. M. Alam, H. Keiko and S. Yusa , "Schizophrenic micelle of a water-soluble diblock polymer and its application to a thermo-optical device," *Colloid Polym Sci,* vol. 292, p. 1611–1617.

[5] D. Patel , K. Kuperkar, S. i. Yusa and P. Bahadur , "Nanoscale Self-Assemblies from Amphiphilic Block Copolymers as Proficient Templates in Drug Delivery," *Drugs and Drug Candidates,* vol. 2, no. 4, pp. 898-922, 2023.

[6] W. H. Abuwatfa, N. M. AlSawaftah and G. A. Husseini, "Chapter 21 - Block copolymer micelles as long-circulating drug delivery vehicles," in *Polymeric Micelles for Drug Delivery*, Woodhead Publishing Series in Biomaterials, 2022, pp. 531-560.

[7] K. Cholkar, A. Patel , A. D. Vadlapudi and A. K. Mitra, "Novel Nanomicellar Formulation Approaches for Anterior and Posterior Segment Ocular Drug Delivery," *Recent Patents on Nanomedicine,* vol. 2, 2012.

[8] Kataoka, K; Harada, A; Nagasaki, Y;, "Block copolymer micelles for drug delivery: Design, characterization and biological significance," *Advanced Drug Delivery Reviews,* vol. 64, pp. 37-48, 2012.

[9] C. Oerlemans, W. Bult , M. Bos, G. Storm , J. F. Nijsen and W. E. Hennik, "Polymeric Micelles in Anticancer Therapy: Targeting, Imaging and Triggered Release," *Pharm Res,* vol. 27, p. 2569–2589, 2010.

[10] M. P. Robin , S. M. Osborne , Z. Pikramenou , J. E. Raymond and R. K. O'Reilly, "Fluorescent Block Copolymer Micelles That Can Self-Report on Their Assembly and Small Molecule Encapsulation," *Macromolecules,* vol. 49, no. 2, p. 653–662, 2016.

[11] A. Raza, T. Rasheed , F. Nabeel , U. Hayat , M. Bilal and H. M. N. Iqbal, "Endogenous and Exogenous Stimuli-Responsive Drug Delivery Systems for Programmed Site-Specific Release," *Molecules,* vol. 24, no. 1117, 2019.

[12] A. S. Abo Dena and I. M. El-Sherbiny, "Chapter 14 - Light- and temperature-responsive polymeric micelles for drug delivery," in *Polymeric Micelles for Drug Delivery*, Woodhead Publishing Series in Biomaterials, 2022, pp. 395-407.

[13] M. Huang, H. Li, W. Ke, J. Li, C. Zhao and Z. Ge, "Finely Tuned Thermo-Responsive Block Copolymer Micelles for Photothermal Effect Triggered Efficient Cellular Internalization," *Macromol. Biosci,* vol. 16, no. 9, pp. 1265-1272, 2016.

[14] M. Nakayama, J. Akimoto and T. Okano, “Polymeric micelles with stimuli-triggering systems for advanced cancer drug targeting,” *J Drug Target,* vol. 22, no. 7, p. 584–599, 2014.

[15] J. Chen , C. Qian, P. Ren , H. Yu, X. Kong , C. Huang , H. Luo and G. Chen , “Light-Responsive Micelles Loaded With Doxorubicin for Osteosarcoma Suppression,” *Front. Pharmacol.,* vol. 12, 2021.

[16] S. Yadav, K. Ramesh, P. Kumar , S. H. Jo, S. I. Yoo, Y. S. Gal, S. H. Park and K. T. Lim, “Near-Infrared Light-Responsive Shell-Crosslinked Micelles of Poly(d,l-lactide)-b-poly((furfuryl methacrylate)-co-(N-acryloylmorpholine)) Prepared by Diels–Alder Reaction for the Triggered Release of Doxorubicin,” *Materials (Basel).,* vol. 14, no. 24, p. Materials (Basel)., 2021.

[17] Y. Liu, W. Wang , J. Yang , C. Zhou and J. Sun, “pH-sensitive polymeric micelles triggered drug release for extracellular and intracellular drug targeting delivery,” *Asian Journal of Pharmaceutical Sciences,* vol. 8, no. 3, pp. 159-167, 2013.

[18] X. Guo, Y. Cheng, X. Zhao , Y. Luo, J. Chen and W. E. Yuan , “Advances in redox-responsive drug delivery systems of tumor microenvironment,” *Journal of Nanobiotechnology volume,* vol. 16, no. 74, 2018.

[19] F.-Z. El-Gamal, M. Elmogy and A. Atwan , “Current trends in medical image registrationand fusion,” *Egyptian Informatics Journal,* vol. 17, no. 1, pp. 99-124, 2016.

[20] S. Hussain , I. Mubeen , N. Ullah, S. S. U. Din Shah, B. A. Kahn , M. Zahoor, R. Ullah , F. A. Khan and M. A. Sultan , “Modern Diagnostic Imaging Technique Applications and Risk Factors in the Medical Field: A Review,” *Biomed Res Int.,* vol. 19, p. 2022, 2022.

[21] D. P. Cormode, P. C. Naha and Z. A. Fayad, “Nanoparticle Contrast Agents for Computed Tomography: A Focus on Micelles,” *Contrast Media Mol Imaging,* vol. 9, no. 1, p. 37–52, 2014.

[22] J. J. Vaquero and P. Kinahan, “Positron Emission Tomography: Current Challenges and Opportunities for Technological Advances in Clinical and Preclinical Imaging Systems,” *Annu Rev Biomed Eng,* vol. 17, p. 385–414, 2015.

[23] S. Goel, C. G. England, F. Chen and W. Cai, “Positron Emission Tomography and Nanotechnology: A Dynamic Duo for Cancer Theranostics,” *Adv Drug Deliv Rev.,* vol. 113, p. 157–176, 2017.

[24] N. R. Nelson , J. D. Port and P. K. Pandey , “Use of Superparamagnetic Iron Oxide Nanoparticles (SPIONs) via Multiple Imaging Modalities and Modifications to Reduce Cytotoxicity: An Educational Review,” *J. Nanotheranostics,* vol. 1, no. 1, pp. 105-135, 2020.

[25] M. Gaeta , M. Cavallaro, S. L. Vinci , E. Mormina , A. Blandino , M. A. Marino , F. Granata , A. Tessitore, K. Galletta, T. D'Anglelo and C. Visalli , “Magnetism of materials: theory and practice in magnetic resonance imaging,” *Insights Imaging,* vol. 12, no. 179, 2021.

[26] V. Jacques , S. Dumas , W. C. Sun, J. S. Troughton , M. T. Greenfield and P. Caravan , “High relaxivity MRI contrast agents part 2: Optimization of inner- and second-sphere relaxivity,” *Invest Radiol,* vol. 45, no. 10, p. 613–624, 2010.

[27] H. Hu, “Recent Advances of Bioresponsive Nano-Sized Contrast Agents for Ultra-High-Field Magnetic Resonance Imaging,” *Front. Chem.,* vol. 8, no. 203, 2020.

[28] Y. D. Xiao, R. Paudel, J. Liu, C. Ma, Z. S. Zhang and S. K. Zhou , “MRI contrast agents: Classification and application (Review),” *International Journal of Molecular Medicine ,* vol. 38, no. 5, pp. 1319-1326, 2016.

[29] N. J. Serkova , “Nanoparticle-Based Magnetic Resonance Imaging on Tumour-Associated Macrophages and Inflammation,” *Front. Immunol,* vol. 8, no. 590, 2017.

[30] Y. Wei , H. Jiang , Q. Li, F. Che , S. Wan , S. Yao , F. Gao, T. Zhang , J. Wang and B. Song , “Multi-nuclear magnetic resonance spectroscopy: state of the art and future directions,” *Insights Imaging,* vol. 13, no. 135, 2022.

[31] Z. Han and G. Liu, “CEST MRI trackable nanoparticle drug delivery systems,” *Biomed Mater.,* vol. 16, no. 2, p. 024103, 2021.

[32] V. Ntziachristos, “Fluorescence Molecular Imaging,” *Annu. Rev. Biomed. Eng.,* vol. 8, pp. 1-33, 2006.

[33] J. Qian , Z. Feng , X. Fan, A. Kuzmin, A. S. Gomes and P. N. Prasad, “High contrast 3-D optical bioimaging using molecular and nanoprobes optically responsive to IR light,” *Physics Reports,* vol. 962, no. 10.1016/j.physrep.2022.02.004, pp. 1-107, 2022.

[34] L. K. Neijenhuis, L. D. Myunck, O. D. Neijenhuis, P. J. Kuppen , D. E. Hiling , F. J. Borm, D. Cohen, J. S. Mieog , W. H. Steup , J. Braun , A. l. Vahrmeijer , A. L. Varmeijer and M. Hutteman, “Near-Infrared Fluorescence Tumor-Targeted Imaging in Lung Cancer: A Systematic Review,” *Life,* vol. 12, no. 3, p. 446, 2022.

[35] Y. L. Balachandran and X. Jiang, “Aggregation-Induced Fluorogens in Bio-Detection, Tumor Imaging, and Therapy: A Review,” *CCS Chemistry,* vol. 4, no. 2, pp. 420-436, 2022.

[36] G. Yeroslavsky, M. Umezawa, K. Okubo , K. Nigoghossian, D. T. Dung , K. Miyata , M. Kamimura and K. Soga , “Stabilization of indocyanine green dye in polymeric micelles for NIR-II fluorescence imaging and cancer treatment,” *Biomater. Sci,* vol. 8, pp. 2245-2254, 2020.

[37] Z. Wang , S. Chen , J. W. Lam , W. Qin , R. T. Kwok, N. Xie , Q. Hu and B. Z. Tang , “Long-Term Fluorescent Cellular Tracing by the Aggregates of AIE Bioconjugates,” *J. Am. Chem. Soc.,* vol. 135, no. 22, p. 8238–8245, 2013.

[38] H. Shi , N. Liang , J. Liu , S. Li , X. Gong , P. Yan and S. Sun , “AIE-active polymeric micelles based on modified chitosan for bioimaging-guided targeted delivery and controlled release of paclitaxel,” *Carbohydrate Polymers,* vol. 118327, 2021.

[39] K. Yan , S. Zhang , K. Zhang , Y. Miao, Y. Qiu, P. Zhang , X. Jia and X. Zhao , “Enzyme-responsive polymeric micelles with fluorescence fabricated through aggregation induced copolymer self-assembly for anticancer drug delivery,” *Polym. Chem.,* vol. 11, pp. 7704-7713, 2020.

[40] B. Kulkarni, S. Qutub , V. Ladelta, N. M. Khashab and N. Hadjichristidis, “AIE-Based Fluorescent Triblock Copolymer Micelles for Simultaneous Drug Delivery and Intracellular Imaging,” *Biomacromolecules,* vol. 22, no. 12, pp. 5243-5255, 2021.

[41] J. Lee, J. H. Im , K. M. Huh, Y. k. Lee and H. Shin, “Preparation and Characterization of CdSe/ZnS Quantum Dots Encapsulated in Poly(ethylene glycol)-b-Poly(D,L-lactide) Micelle Nanoparticles,” *Journal of Nanoscience and Nanotechnology,* vol. 10, p. 487–496, 2010.

[42] H. Y. Yang, Y. Fu, M. S. Jang , Y. Li, W. P. Yin , T. K. Ahn , J. H. Lee, H. Chae and D. S. Lee, “CdSe@ZnS/ZnS quantum dots loaded in polymeric micelles as a pH-triggerable targeting fluorescence imaging probe for detecting cerebral ischemic area,” *Colloids and Surfaces B: Biointerfaces,* vol. 155, pp. 497-506, 2017.

[43] T. Yu, W. Zhuang , X. Su, B. Ma, J. Hu, H. He, G. Li and Y. Wang , “Dual-Responsive Micelles with Aggregation-Induced Emission Feature and Two-Photon Aborsption for Accurate Drug Delivery and Bioimaging,” *Bioconjugate Chem,* vol. 30, no. 7, p. 2075–2087, 2019.

[44] I. Chandrasiri , D. G. Abebe, M. K. Yaddehige , J. S. Williams , M. F. Zia , A. Dorris, A. Barker , B. L. Simms , A. Parker , B. P. Vinjamuri, N. Le, J. N. Gayton , M. B. Chougule , N. I. Hammer , A. Flynt , J. H. Delcamp and D. L. Watkins , “Self-Assembling PCL–PAMAM Linear Dendritic Block Copolymers (LDBCs) for Bioimaging and Phototherapeutic Applications,” *ACS Appl. Bio Mater,* vol. 3, no. 9, p. 5664–5677, 2020.

[45] C. M. Ellis, D. Yuan , F. E. Mózes, J. J. Miller and J. J. Davis , “Reversible pH-responsive MRI contrast with paramagnetic polymer micelles,” *Chem. Commun.,* vol. 59, no. 12, pp. 1605-1608, 2023.

[46] K. Shiraishi , K. Kawano, Y. Maitani and M. Yokoyama , “Polyion complex micelle MRI contrast agents from poly(ethylene glycol)-b-poly(l-lysine) block copolymers having Gd-DOTA; preparations and their control of T1-relaxivities and blood circulation characteristics,” *Journal of Controlled Release,* vol. 148, no. 2, pp. 160-167, 2010.

[47] G. Hong , J. x. Zhou and R. x. Yuan, “Folate-targeted polymeric micelles loaded with ultrasmall superparamagnetic iron oxide: combined small size and high MRI sensitivity,” *Int J Nanomedicine,* vol. 7, p. 2863–2872, 2012.

[48] E. Nakamura , K. Makino, T. Okano , T. Yamamoto and M. Yokoyama , “A polymeric micelle MRI contrast agent with changeable relaxivity,” *Journal of Controlled Release,* vol. 114, no. 3, pp. 325-333, 2006.

[49] K. M. Bennett, J. i. Jo, H. Cabral , R. Bakalova and I. Aoki, “MR imaging techniques for nano-pathophysiology and theranostics,” *Advanced Drug Delivery Reviews,* 2014.

[50] C. Wu, D. Li, L. Yang , B. Lin , H. Zhang , Y. Xu, Z. Cheng, C. Xia, Q. Gong , B. Song and H. Ai, “Multivalent manganese complex decorated amphiphilic dextran micelles as sensitive MRI probes,” *J. Mater. Chem. B,* vol. 3, no. 1470, 2015.

[51] A. Mali, E. L. Kaijzel, H. J. Lamb and L. J. Cruz, “19F-nanoparticles: Platform for in vivo delivery of fluorinated biomaterials for 19F-MRI,” *Journal of Controlled Release,* vol. 338, pp. 870-889, 2021.

[52] W. Du, A. M. Nystrom, L. Zhang, K. T. Powell, Y. Li, C. Cheng, S. A. Wickline and K. L. Wooley, “Amphiphilic Hyperbranched Fluoropolymers as Nanoscopic 19F Magnetic Resonance Imaging Agent Assemblies,” *Biomacromolecules,* vol. 9, p. 2826–2833, 2008.

[53] O. Koshkina, T. Rheinberger, V. Flocke , A. Windfelder, P. Bouvain, N. M. Hamelmann, J. M. Paulusse, H. Gojzewski, U. Flögel and F. R. Wurm, “Biodegradable polyphosphoester

micelles act as both background-free 31P magnetic resonance imaging agents and drug nanocarriers," *Nature Communications,* vol. 14, p. 4351, 2023.

[54] S. Zhang , K. Zhou , G. Huang, M. Takahashi , A. D. Sherry and J. Gao, "A novel class of polymeric pH-responsive MRI CEST agents," *Chem. Commun.,* vol. 49, p. `6418, 2013.

[55] C. Wang , S. Ravi, G. V. Martinez, V. Chinnasamy , P. Raulji, M. Howell , Y. Davis , J. Mallela, M. S. Seehra and S. Mohapatra, "Dual-purpose magnetic micelles for MRI and gene delivery," *Journal of Controlled Release,* vol. 163, no. 1, pp. 82-92, 2012.

[56] X. Li, Y. Qian , T. Liu, X. Hu, G. Zhang , Y. You and S. Liu , "Amphiphilic multiarm star block copolymer-based multifunctional unimolecular micelles for cancer targeted drug delivery and MR imaging," *Biomaterials,* vol. 32, no. 27, pp. 6595-6605, 2011.

[57] X. Hu, G. Liu, Y. Li, X. Wang and S. Liu, "Cell-Penetrating Hyperbranched Polyprodrug Amphiphiles for Synergistic Reductive Milieu-Triggered Drug Release and Enhanced Magnetic Resonance Signals," *J. Am. Chem. Soc.,* vol. 137, no. 1, p. 362–368, 2015.

[58] A. I. Jensen , T. Binderup , P. K. Ek, C. E. Grandjean, P. H. Rasmussen , A. Kjær and T. L. Andresen, "PET imaging with copper-64 as a tool for real-time in vivo investigations of the necessity for cross-linking of polymeric micelles in nanomedicine," *J Label Compd Radiopharm.,* vol. 60, p. 366–374, 2017.

[59] J. Yang , W. Lu, J. Xiao, Q. Zong , H. Xu, Y. Yin, H. Hong and W. Xu, "A positron emission tomography image-guidable unimolecular micelle nanoplatform for cancer theranostic applications," *Acta Biomaterialia,* vol. 79, pp. 306-316, 2018.

[60] D. P. Cormode , P. C. Naha and Z. A. Fayad , "Nanoparticle contrast agents for computedtomography: a focus on micelles," *Contrast Media Mol. Imaging,* vol. 9, pp. 37-52, 2014.

[61] P. Zhang, X. Ma, R. Guo, Z. Ye, H. Fu, N. Fu, Z. Guo, J. Zhang and J. Zhang, "Organic Nanoplatforms for Iodinated Contrast Media in CT Imaging," *Molecules,* vol. 26, no. 23, p. 7063, 2021.

[62] J. Balegamire, M. Vandamme, E. Chereul , S. Si-Mohamed, S. A. Maache , E. Almouazen, L. Ettouati, H. Fessi, L. Boussel , P. Douek and Y. Chevalier , "Iodinated polymer nanoparticles as contrast agent for spectral photon counting computed tomography," *Biomater. Sci.,* vol. 8, pp. 5715-5728, 2020.

[63] C. Tang, A. W. York , J. L. Mikitsh , A. C. Wright , A. M. Chacko, D. R. Elias , Y. Xu, H. K. Lim and R. K. Prud'homme, "Preparation of PEGylated Iodine-Loaded Nanoparticles via Polymer-Directed Self-Assembly," *Macromol. Chem. Phys.,* vol. 219, p. 1700592, 2018.

[64] W. Zhou , Y. Chen , Y. Zhang , X. Xin, R. Li, C. Xie and Q. Fan , "Iodine-Rich Semiconducting Polymer Nanoparticles for CT/Fluorescence Dual-Modal Imaging-Guided Enhanced Photodynamic Therapy," *Small,* vol. 16, no. 1905641, 2020.

[65] W. J. Li, Y. Wang , Y. Liu, T. Wu, W. L. Cai, X. T. Shuai and G. B. Hong , "Preliminary Study of MR and Fluorescence Dual-mode Imaging: Combined Macrophage-Targeted and Superparamagnetic Polymeric Micelles," *Int. J. Med. Sci.,* vol. 15, no. 2, pp. 129-141, 2018.

[66] L. W. Starmans, M. A. Hummelink, R. Rossin , E. C. Kneepkens, R. Lamerichs, K. Donato, K. Nicolay and H. Grüll, “89 Zr- and Fe-Labeled Polymeric Micelles for Dual Modality PET and T 1 -Weighted MR Imaging,” *Adv. Healthcare Mater,* vol. 4, p. 2137–2145, 2015.